

FMH606 Master's Thesis 2020

Process Technology

# **Computational modeling of fluidized bed behavior with agglomerates**

Krister Jakobsen

Faculty of Technology, Natural sciences and Maritime Sciences  
Campus Porsgrunn

**Course:** FMH606 Master's Thesis, 2020

**Title:** Computational modeling of fluidized bed behavior with agglomerates.

**Number of pages:** 83

**Keywords:** Bubbling Fluidized bed, Glicksman's scaling rules, Computational Particle Fluid Dynamic (CPFD), Agglomerates

**Student:** Krister Jakobsen

**Supervisors:** Britt M. E. Moldestad, Nora C. I. S. Furuvik (Co-supervisor)

**Availability:** Open

**Summary:**

The transition towards the use of more renewable energy is an essential subject for the imminent climate crisis. Biomass can be converted into syngas in a gasification process. The formation of agglomerates in a Bubbling Fluidized Bed (BFB) gasifier is a major problem when gasifying biomass to syngas. An agglomerated bed may lead to instability in the fluidization process. These instabilities are incomplete fluidization, fluid channeling, and defluidized zones in the gasifier. In the worst cases, agglomeration may lead to complete defluidization of the bed. The objective of this thesis is to develop a Computational Particle Fluid Dynamic (CPFD) model to simulate the flow behavior in a hot BFB with agglomerates.

The CPFD model is created using the commercial software Barracuda Virtual Reactor 17.4.1 and validated with experiments performed in both cold and hot models of BFB. The models showed promising accuracy when compared with the experimental data. The cold and hot BFB had an average deviation of 6 %, and a deviation of 3 %, respectively. The minimum fluidization velocity for the cold and hot model was 6 % and 12 %, respectively. The hot BFB geometry was scaled up from lab-scale to pilot-scale using Glicksman's scaling rules. The pilot-scaled bed needed additional agglomerates corresponding to 20% of the bed volume to affect the flow behavior.

The agglomerated bed simulation gave promising results. The simulation showed similarities in the flow behavior with experimental data found in the literature. The overall pressure gradient over the bed decreased, and the minimum fluidization velocity increased. The CPFD model is capable of predicting the fluidization process in a BFB gasifier with agglomerates.

# Preface

This thesis is written in the spring semester of 2020 as a final assignment in the field of study Process Technology at the University of Southeast Norway.

I would like to thank the following persons for their help:

Britt M. E. Moldestad and Nora C. I. S Furuviik for supervising me and guiding me through the research work. I also would like to thank Rajan Jaiswal for helping me with simulations and experiments.

Porsgrunn, 2020

Krister Jakobsen

# Contents

Preface .....	3
Contents.....	4
Figure List.....	6
Table List .....	9
Nomenclature .....	10
<b>1 Introduction .....</b>	<b>13</b>
1.1 Background .....	13
1.2 Objectives.....	14
1.3 Overview and Scope.....	15
<b>2 Biomass Gasification.....</b>	<b>16</b>
2.1 Gasification Process .....	16
2.2 Gasification Technologies .....	18
2.2.1 <i>Bubbling Fluidized Bed Parameters</i> .....	20
2.3 Principle of Gasification Reactions .....	22
2.4 Agglomeration in a Bubbling Fluidized Bed .....	25
<b>3 Scaling of Bubbling Fluidized Bed Reactor .....</b>	<b>28</b>
3.1 Glicksman's Rule of Scaling.....	28
<b>4 Experimental Work.....</b>	<b>30</b>
4.1 Cold-BFB .....	30
4.1.1 <i>Sieve Analysis</i> .....	31
4.1.2 <i>Bed Parameters Descriptions</i> .....	32
4.1.3 <i>Experimental Results</i> .....	33
4.2 BFB-Gasifier .....	35
4.2.1 <i>Bed Parameters Descriptions</i> .....	36
4.2.2 <i>Experimental Results</i> .....	37
<b>5 CPFD Model Development .....</b>	<b>39</b>
5.1 Computational Fluid Dynamic .....	39
5.2 Barracuda .....	40
5.2.1 <i>Global Setting and Base Material</i> .....	40
5.2.2 <i>Particle Description</i> .....	40
5.2.3 <i>Set-up Grid</i> .....	41
5.2.4 <i>Initial Conditions</i> .....	44
5.2.5 <i>Boundary Conditions</i> .....	45
5.2.6 <i>Numerics</i> .....	46
5.2.7 <i>Time Controls</i> .....	46
5.2.8 <i>Data Outpoints and Post-run</i> .....	46
5.3 Cold-BFB Model .....	48
5.3.1 <i>Testing of Various Drag Models</i> .....	48
5.3.2 <i>Testing of Various Parameters</i> .....	53
5.4 BFB-Gasifier Model.....	58
5.5 Set-Up For Insertion of Agglomerates.....	61
5.5.1 <i>Bed Parameters and CPFD Parameters for the Pilot-Scale</i> .....	61

*5.5.2 Confirming the Pilot-Scaled Gasifier* ..... 63  
*5.5.3 Injection Set-Up*..... 64

**6 Results and Discussion**..... 66

6.1 Comparison Between Experimental and Simulated Results..... 66  
6.2 Results From Agglomerated Bed..... 68

**7 Conclusion** ..... 75

**References**..... 76

**Appendices**..... 78

# Figure List

Figure 2.1: The chain of steps in a gasification process. [5].....	16
Figure 2.2: Illustration of the two bed categorizations with different configurations. [5].....	19
Figure 2.3: Graphical localization of minimum fluidization velocity in a pressure gradient vs. velocity plot. [15].....	21
Figure 2.4: Ideal textbook behavior in a bed with uniformly sized sand represented in a pressure drop ( $\Delta p$ ) vs. superficial velocity ( $u_0$ ) plot. [13] .....	22
Figure 2.5: Peat vs. hardwood under gasification in steam compared in a conversion diagram. [5].....	23
Figure 2.6: Agglomerates from fluidized bed biomass gasification. ....	26
Figure 2.7: Fluidized bed bubbling frequency, both with and without agglomerates. [18].....	26
Figure 2.8: BFB experiment with no agglomerates (I) and with agglomerates at the bottom of the bed (II). [15].....	27
Figure 2.9: BFB experiment with agglomerates at the bottom (II) and top (III) of the bed. [15] .....	27
Figure 4.1: Experiment, Cold-BFB: the layout, set up, and dimensions for the column. [22]	30
Figure 4.2: Laboratory sieves. [23].....	31
Figure 4.3: Sieve shaker. [24].....	31
Figure 4.4: Experiment, Cold-BFB: experimental data displayed in a pressure gradient vs. superficial velocity plot with the locations of minimum fluidization velocities. ....	34
Figure 4.5: Experiment, BFB-gasifier: set up viewed from the right side.....	35
Figure 4.6: Experiment, BFB-gasifier: set up viewed from the left side. ....	35
Figure 4.7: Experiment, BFB-gasifier: layout and dimensions. [26].....	36
Figure 4.8: Experiment, BFB-gasifier: experimental results plotted in a pressure gradient (Pa/m) vs. superficial velocity (m/s). ....	38
Figure 5.1: Parameter, Cold-BFB model: PSD sheet. ....	41
Figure 5.2: Barracuda: built-in agglomeration function. ....	41
Figure 5.3: Cold-BFB model: CAD geometry.....	42
Figure 5.4: Cold-BFB: The provided grid check tool from Barracuda.....	43
Figure 5.5: Cold-BFB: grid layout presented in 2-D. ....	43
Figure 5.6: Cold-BFB: grid layout presented in 3-D. ....	44
Figure 5.7: Cold-BFB: layout for the boundary conditions. ....	45
Figure 5.8: Cold-BFB: pressure sensor location in the geometry.....	47
Figure 5.9: Drag model test, Cold-BFB model: drag models compared to each other.....	51

Figure 5.10: Drag model test, Cold-BFB model: drag models compared to each other, including "Experiment Cold-BFB".....	52
Figure 5.11: Drag model test, Cold-BFB model: selected drag models compare with the experimental results for Cold-BFB, including the locations of minimum fluidization velocities.....	52
Figure 5.12: Parameter test, Cold-BFB model: increased close pack volume fraction compared with Base Case and experimental data.....	53
Figure 5.13: Parameter test, Cold-BFB model: extended fluid velocity duration compared with Base Case and experimental data.....	54
Figure 5.14: Parameter test, Cold-BFB model: decrease normal to wall retention compared with Base Case and experimental data.....	54
Figure 5.15: Parameter test, Cold-BFB model: lower grid resolution compared with Base Case and experimental data.....	55
Figure 5.16: Parameter test, Cold-BFB model: Relocation of pressure sensors compared with Base Case and experimental data.....	56
Figure 5.17: Parameter test, Cold-BFB model: decreased timestep compared with Base Case and experimental data.....	56
Figure 5.18: Parameter test, Cold-BFB model: finder grid resolution with decreased timestep compared with Base Case and experimental data.....	57
Figure 5.19: Parameter test, Cold-BFB model: PSD test, which includes a more narrowed size distribution and a mean particle size compared with Base Case and experimental data.....	58
Figure 5.20: BFB-gasifier: grid layout presented in 2-D.....	59
Figure 5.21: BFB-gasifier: pressure sensor locations in the geometry.....	60
Figure 5.22: Parameter, BFB-gasifier: PSD sheet.....	60
Figure 5.23: Simulation, BFB-gasifier: simulated data compared with the experimental data from the BFB-gasifier.....	61
Figure 5.24: Pilot-Scaled Gasifier: grid layout presented in 2-D.....	63
Figure 5.25: Simulation, Pilot-Scaled Gasifier: simulated data with the localization of the minimum fluidized velocity.....	64
Figure 5.26: Parameter, Pilot-Scaled Gasifier: used injection settings in Barracuda.....	64
Figure 5.27: Pilot-Scale Gasifier: injection location in the geometry with nozzle direction...	65
Figure 6.1: Result, Cold-BFB model: model validation with the locations of minimum fluidization velocities.....	66
Figure 6.2: Result, BFB-gasifier: model validation with the location of minimum fluidization velocity.....	67
Figure 6.3: Result, Pilot-Scale Gasifier: comparison between simulation with and without agglomerates at a constant velocity.....	68
Figure 6.4: Result, Pilot-Scale Gasifier: injection at time 0 s.....	69

Figure 6.5: Result, Pilot-Scale Gasifier: injection at time 8 s.....	69
Figure 6.6: Result, Pilot-Scale Gasifier: injection at time 52 s.....	69
Figure 6.7: Result, Pilot-Scale Gasifier: injection at time 60 s.....	69
Figure 6.8: Result, Pilot-Scale Gasifier: injection at time 90 s.....	69
Figure 6.9: Result, Pilot-Scale Gasifier: particle volume fraction at injection time 14 s. ....	70
Figure 6.10: Result, Pilot-Scale Gasifier: particle volume fraction at injection time 52 s. ....	70
Figure 6.11: Result, Pilot-Scale Gasifier: particle volume fraction at injection time 60 s. ....	70
Figure 6.12: Result, Pilot-Scale Gasifier: particle volume fraction at injection time 90 s. ....	70
Figure 6.13: Result, Pilot-Scale Gasifier: comparison between the agglomerated bed and the normal bed. Points of minimum fluidization velocities are included. ....	71
Figure 6.14: Result, Pilot-Scale Gasifier: species at minimum fluidization velocity of 0.055 m/s.....	73
Figure 6.15: Result, Pilot-Scale Gasifier: particle volume fraction at minimum fluidization velocity of 0.055 m/s.....	73
Figure 6.16: Result, Pilot-Scale Gasifier: particle volume fraction without agglomerates at a gas velocity of 0.085 m/s .....	73
Figure 6.17: Result, Pilot-Scale Gasifier: particle volume fraction with agglomerates at a gas velocity of 0.085 m/s.....	73
Figure 6.18: Result, Pilot-Scale Gasifier: at a gas velocity of 0.101 m/s. ....	74
Figure 6.19: Result, Pilot-Scale Gasifier: particle volume fraction without agglomerates at a gas velocity of 0.101 m/s. ....	74
Figure 6.20: Result, Pilot-Scale Gasifier: particle volume fraction, at a gas velocity of 0.101 m/s.....	74
Figure 6.21: Result, Pilot-Scale Gasifier: at a gas velocity of 0.37 m/s. ....	74
Figure 6.22: Result, Pilot-Scale Gasifier: particle volume fraction, at a gas velocity of 0.37 m/s.....	74



# Table List

Table 2.1: Some fuel products from biomass presented in each phase of matter. [5] .....	17
Table 2.2: Some products from pyrolysis of biomass presented in each phase of matter. [5]	17
Table 2.3: Chemical reactions in a gasification process represented with the heat of reaction at 25°C. [5].....	24
Table 2.4: Gasifying mediums reaction rate represented as an order of magnitude.[5] .....	25
Table 2.5: Ash melting temperature for three different biomasses. [10] .....	25
Table 4.1: Experiment, Cold-BFB: calculated bed parameters. ....	32
Table 4.2: Experiment, Cold-BFB: corrected bed parameters.....	33
Table 4.3: Experiment, Cold-BFB: volumetric flow rate converted to linear velocity. ....	33
Table 4.4: Experiment, BFB-gasifier: parameters for the mass flow rate to linear velocity conversion.....	37
Table 4.5: Experiment, BFB-gasifier: calculated bed parameters. ....	37
Table 5.1: Parameter, Cold-BFB model: Boundary condition, the initial flow chart.....	46
Table 5.2: Parameter, Cold-BFB model: pressure sensor coordinates. ....	47
Table 5.3: Wen-Yu drag model parameters at the default value. [28].....	49
Table 5.4: Ergun drag model parameters at the default value. [28].....	49
Table 5.5: WenYu-Ergun drag model blend, parameter explanation. [28] .....	50
Table 5.6: Turton-Levenspiel drag model parameters at the default value. [28].....	50
Table 5.7: Non-spherical Haider-Levenspiel drag model parameters at the default value. [28] .....	51
Table 5.8: Parameter test, Cold-BFB model: new coordinates for pressure sensors.....	55
Table 5.9: Parameter, BFB-gasifier: pressure sensor coordinates. ....	59
Table 5.10: Glicksman's scaling parameters: BFB-gasifier to Pilot-Size dimensions. ....	62
Table 5.11: Parameter, Pilot-Scaled Gasifier: pressure sensor coordinates.....	63

# Nomenclature

<b>Abbreviations/expressions</b>	<b>Explanations</b>	<b>Unit</b>
BFB	Bubbling Fluidized Bed	
BC	Boundary Condition	
CFB	Circulating Fluidized Bed	
CFD	Computational Fluid Dynamic	
CPFD	Computational Particle Fluid Dynamic	
CPVF	Close Pack Volume Fraction	
DPM	Discrete Parcel Method	
IC	Initial Conditions	
PSD	Particle Size Distribution	
MP-PIC	Multiphase Particle-In-Cell	
NLPM	Normal Liter Per Minute	
WF	Weight Fraction	

<b>Unit of measurement</b>	<b>Explanations</b>	<b>SI Unit</b>
$C_d$	Drag coefficient	[-]
$D$	Column diameter	[m]
$D_f$	Drag Function	[1/s]
$d_p$	Particle diameter	[m]
$F_p$	Force acted on particle	[kg.m/s <sup>2</sup> ]
$g$	Gravital acceleration	[m/s <sup>2</sup> ]
$H$	Column height	[m]
$h$	Bed height	[m]
$L$	Length dimension	[m]

			Nomenclature
$m_p$	Particle mass	[kg]	
P	Pressure sensor	[-]	
p	Pressure	[Pa]	
$r_p$	Particle radius	[m]	
Re	Reynold number	[-]	
$Re_{mf}$	Reynold number at minimum fluidization velocity	[-]	
T	Temperature	[K]	
$u_{mb}$	Minimum bubbling velocity	[m/s]	
$u_{mf}$	Minimum fluidization velocity	[m/s]	
$u_0$	Superficial velocity	[m/s]	
<b>Greek letters</b>	<b>Explanations</b>	<b>Unit</b>	
$\varepsilon$	Void	[-]	
$\varepsilon_m$	Void at fixed bed	[-]	
$\varepsilon_{mf}$	Void at minimum fluidization velocity	[-]	
$\theta_{CP}$	Close pack volume fraction	[-]	
$\theta_f$	Fluid volume fraction	[-]	
$\theta_p$	Particle volume fraction	[-]	
$\mu_g$	Gas viscosity	[Pa.s]	
$\rho$	Density	[kg/m <sup>3</sup> ]	
$\rho_{bulk}$	Bulk density	[kg/m <sup>3</sup> ]	
$\rho_g$	Gas density	[kg/m <sup>3</sup> ]	
$\rho_p$	Particle density	[kg/m <sup>3</sup> ]	
$\Phi$	Particle Sphericity	[-]	

<b>Chemical compound</b>	<b>Explanations</b>	<b>Unit</b>
CH <sub>4</sub>	Methane	
C <sub>2</sub> H <sub>4</sub>	Ethylene	
C <sub>2</sub> H <sub>6</sub>	Ethane	
C <sub>6</sub> H <sub>6</sub>	Benzene	
CO	Carbon Monoxide	
CO <sub>2</sub>	Carbon dioxide	
H <sub>2</sub>	Hydrogen	
H <sub>2</sub> O	Water	
O <sub>2</sub>	Oxygen	

# 1 Introduction

This chapter addresses the background, the objectives, and the scope.

## 1.1 Background

The transition towards the use of more renewable energy is an essential subject for the imminent climate crisis. As the global energy demand is gradually increasing, a drive to use a more sustainable energy source than fossil fuel is essential for the future. Biomass is considered a renewable energy source and is more sustainable than fossil fuel. [1]-[3]

Syngases is extracted from biomass through a thermochemical process known as gasification. A fluidized bed reactor is used for gasification, to ensure proper mixing of biomass and fluidizing gas, and thus higher heat transfer and more uniform temperature in the reactor. [4]

Using fluidized beds offer both advantages and disadvantages when performing gasification. Some of the advantages are listed above, and the disadvantages are that agglomerates can be formed. Agglomerates are created from the bed materials and the inorganic components from biomass. Under high-temperature operations, the alkali metals, which are present in biomass ash, reacts with the bed material, and create agglomerates. Agglomeration may disrupt the flow in the fluidized bed and thus affect the overall efficiency in the bed. [5]

## 1.2 Objectives

Agglomerates are generated when char is gasified at high temperatures. The ash melts and becomes a sticky glue. This stickiness can make the bed materials lump together and agglomerate. The objective is to be able to simulate the operating parameters in the fluidized bed when agglomerates are present. Then create a model that can predict the flow behavior of an agglomerated bed. The model is created through experimental and computational methods. Computational Particle Fluid Dynamic (CPFD) is used to create the computational model for the study. The following achievements state the main objective:

1. Literature survey:
  - Get a general understanding of gasification and the various steps and set-ups.
  - Get a general understanding of how agglomerates are created and how they affect a bubbling fluidized bed (BFB).
  - Get a general understanding of how to scale various reactors from lab-scale to pilot-scaled.
2. Performing experiments to find out the pressure gradient and minimum fluidization over a cold and hot BFB.
3. Develop a CPFD model through comparison and validation with a cold and hot experimental BFB model.
  - Drag model tests:
    - i. Wen-Yu
    - ii. Ergun
    - iii. WenYu-Ergun
    - iv. Turton-Levenspiel
    - v. Non-Spherical
  - Parameter tests:
    - i. Close Pack Volume Fraction (CPVF)
    - ii. Transient duration for each fluid velocity
    - iii. Timestep
    - iv. Grid resolutions
    - v. Pressure transient point locations
    - vi. Sand Particle Size Distribution (PSD)
4. Utilize the validated CPFD model to simulate the flow behavior with an agglomerated bed.
  - Main tasks to achieve:
    - i. Up-scale the lab-scaled gasifier to a pilot-scaled gasifier with the Glicksman's method and validate the scale.
    - ii. Find the amount of agglomerates needed to affect the flow behavior in the bed.
    - iii. Simulate with the found amount of agglomerates and see the behavior in the BFB.
    - iv. Compare the behavior of simulated results with existing experimental results.

### 1.3 Overview and Scope

It is performed an investigation on how agglomerates affect the flow behavior in a fluidized bed through simulation and literature study. A CPFD model is developed and validated through a data comparison between a computational tool and lab-scaled experimental models. The experimental models are both cold and hot bubbling fluidized beds. The experimental hot BFB model is scaled up to a pilot-scale for the CPFD model to function with agglomerates. The pilot-scaled gasifier is then simulated with an agglomerated bed, then analyzed and compared with the literature study.

Chapter 2 covers a detailed literature study on the gasification process and how agglomerate is formed. The literature study also includes how agglomerates affect the flow behavior and the stability in a bubbling fluidized bed.

Chapter 3 explains Glicksman's rules of scaling.

Chapter 4 includes both a detailed explanation of the experimental set-ups and a presentation of the results gathered from the experiments.

Chapter 5 covers four subjects. First is a short explanation of what CPFD is, second is a cover of the parameter used when creating the model, third covers the various model tests, and fourth utilizes all the previous subjects to create a model that may simulate the behavior of an agglomerated bed.

Chapter 6 presents the simulated results from the experiments for validation and the agglomerated bed. There is also included discussion alongside the presented results.

Chapter 7 covers the conclusion found through simulations and literature review.

## 2 Biomass Gasification

This chapter covers the main concepts in a biomass fluidized bed gasifier and how agglomerates are created. The chapter is also addressing BFB parameters and the effect that an agglomerated bed has on the flow behavior for a BFB.

### 2.1 Gasification Process

Gasification is a series of chemical reactions where hydrogen and carbon monoxide are produced from organic composed material with a restricted supply of oxygen. This product composition is also known as syngas. Gasification can be performed on various hydrocarbon-containing materials, including coal, waste, and biomass. Gasification carries similarities to combustion but varies in the aspect of energy conservation. Gasification packs energy into chemical bonds, while combustion breaks them to release energy. [4]-[6]

The gasification process of biomass typically includes a chain of steps. These gasification steps include drying, pyrolysis, combustion, and gasification, as illustrated in Figure 2.1. [5]

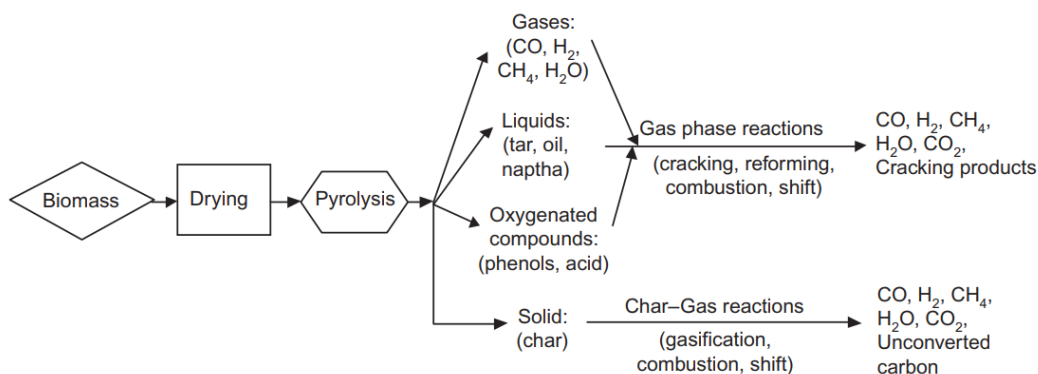


Figure 2.1: The chain of steps in a gasification process. [5]

Biomass is organic material that has been formed from the plant's and animal's circle of life. Thus, instead of waiting millions of years for this to become fossil fuels, it can be used right away. [5][7]

Biomass can produce three different types of primary fuels. These are liquid fuels, gaseous fuels, and solid fuels, the variety is shown in Table 2.1. The fuels are organic, and if produced from biomass, viewed as renewable. [5]



Table 2.1: Some fuel products from biomass presented in each phase of matter. [5]

Phase	Fuel Products
• Liquid	<i>Ethanol, methanol, biodiesel, vegetable oil, and pyrolysis oil.</i>
• Gaseous	<i>Biogas(CH<sub>4</sub>, CO<sub>2</sub>), substitute natural gas(CH<sub>4</sub>), and syngas(CO, H<sub>2</sub>).</i>
• Solid	<i>Charcoal, torrefied biomass, and char(biochar)</i>

Drying includes the removal of moisture that the biomass contains. A high amount of moisture uses more energy from the gasifier to vaporize the water before the gasification starts, thus higher energy loss/usage. [5]

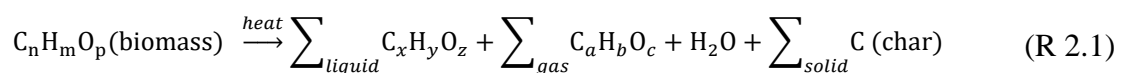
Pyrolysis is, in general, a thermochemical decomposition of biomass. The process can be viewed as similar to devolatilization, carbonization, torrefaction, destructive distillation, and thermolysis. Pyrolysis is a process where noncondensable gases, solid char, and liquid product is created at high temperatures under a specified time with the absence of oxygen. Pyrolysis three principle types of products are shown in Table 2.2. [5][7]

Table 2.2: Some products from pyrolysis of biomass presented in each phase of matter. [5]

Phase	Composition
• Liquid	<i>Tars, heavier hydrocarbons, and water</i>
• Gaseous	<i>e.g., CO<sub>2</sub>, H<sub>2</sub>O, CO, C<sub>2</sub>H<sub>4</sub>, C<sub>2</sub>H<sub>6</sub>, C<sub>6</sub>H<sub>6</sub></i>
• Solid	<i>Char and carbon</i>

Pyrolysis can be divided into two broad classifications: Fast and slow pyrolysis, which is based on the heating rate. Fast pyrolysis has fast pyrolysis reaction time and tends to create bio-oil and gas. Slow pyrolysis has a slow pyrolysis reaction time and usually is used to create char. [5]

Pyrolysis is an important pre-step for a gasification process and can be represented by a generic reaction such as reaction (R 2.1). [5]



Gasification shares similarities with pyrolysis and torrefaction. But pyrolysis and torrefaction do not use any medium to initiate the decomposition process. Gasification needs a medium to initiate the process to rearrange the molecular structure of the biomass. The medium is used to convert solid biomass into favorable gases and liquids. [5]

From Prabir Basu [5]:

## 2 Biomass Gasification

*“The use of a medium is essential for the gasification process, which is not the case for pyrolysis or torrefaction.”*

Gasifying medium is used to react with carbon and heavier hydrocarbons. The medium can convert the carbon and hydrocarbon into CO and H<sub>2</sub> gases, which is categorized as low-molecular-weight gases. The three mainly used gasifying mediums are:

- Oxygen
- Air
- Steam

Oxygen is often the favorable gasifying medium to use, as it can control if the reaction is combustion or gasification. The products of oxygen as a gasifying medium are CO with a low amount of oxygen and carbon dioxide (CO<sub>2</sub>) with a high amount. When there is an excessive amount of oxygen in the air-fuel ratio, then the process moves from gasification to combustion and the products go from “fuel gas” to “flue gas”. The flue gas is not wanted in gasification because it has no heating value. [5]

The oxygen can be supplied to the gasifier in the form of pure oxygen or air. If air is used, then the nitrogen in the air may also influence the product stream. The nitrogen can dilute the product gas and reduce its heating value. If steam is used, then the product may have more hydrogen per unit of carbon and is often presented as an H/C ratio. [5]

### 2.2 Gasification Technologies

The two common biomass gasifiers are categorized as either fixed beds or fluidized beds. Both the categorizations are presented in Figure 2.2, where the updraft and downdraft are two examples of a fixed bed (a). Bubbling bed and circulating bed are configurations of fluidized beds (b). The two latter are also known as Bubbling Fluidized Bed and Circulating Fluidized Bed (CFB). [8]

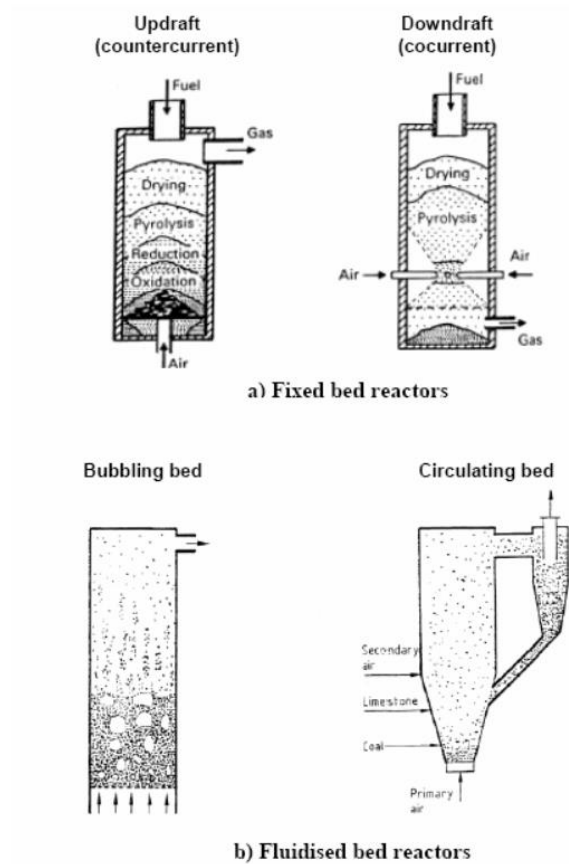


Figure 2.2: Illustration of the two bed categorizations with different configurations. [5]

In the updraft gasifier, fuel or biomass is fed at the top of the reactor. The biomass is then going through the gasification process as it is moving downwards. The reduction and oxidation zones from Figure 2.2 are gasification and combustion, respectively. The air is supplied through a grate at the bottom of the reactor. The supplied air is then traveling upwards and interacting with the hot char. When hot char and air interact, combustion occurs. The combustion forms gaseous products that interact with the biomass. The interaction is in the form of heating and drying the biomass. The closer the biomass is to the combustion, the lesser oxygen, and the higher temperature is present. These conditions are ideal for biomass to undergo pyrolysis. After pyrolysis, comes the gasification zone before it ends in the combustion zone. The product gases are exiting at the top of the bed, while the ash accumulates at the bottom. This technology tends to produce more tars in the gaseous product, compared to the other configurations. [5]-[8]

Another type of fixed bed is a downdraft gasifier, where the air and the biomass are traveling in the same direction inside the bed. The combustion zone is in the center of the bed, making the biomass entering a drying zone then a pyrolysis zone as it travels downwards. After the biomass has left the combustion zone, it is in the gasification zone. The fluid flow is traveling downwards and out. That results in the product gases accompanying the fluid flow and thus travels through a hot zone. The product gases leave the hot zone and the gasifier with a temperature around 1000 °C. In downdraft gasifiers, tars that accompany the gas tends to

## 2 Biomass Gasification

undergo cracking when occupied in the hot zone. The downdraft configuration tends to leave less tar in the product gas, than what the updraft configuration do. [5]-[8]

A Fixed-bed lacks the ability to create a well-mixed environment for good contact between gas and solids, and a uniformly distributed temperature. These abilities give the excellent heat and mass transfer qualities that fluidized-bed has. A Fixed-bed gasifier is also prone to get agglomeration when used with fuels that have a high potential of forming agglomerates. A Fluidized-bed utilizes a fluidized mixture of inert bed material and air to generate an environment for biomass to undergo the necessary steps in gasification. Between the fluidized-bed configurations, CFB enables a more turbulent mixing in the reactor than its counterpart BFB. The CFB system is usually accompanied with a riser and cyclone. The cyclone separates solid particles from the gas stream and returns the particles to the base of the riser. [5]-[8]

### 2.2.1 Bubbling Fluidized Bed Parameters

BFBs are a very crucial technology, especially operations where gas-solid mixing is essential. The fluidized bed gasifier usually operates with a bed temperature around 800-1000 °C, and 900°C for biomass. A bubbling fluidized bed with dense bed material has regions in the bed where there is low solid density, and these regions are called voids ( $\epsilon$ ) or bubbles. The void can control the gross particle movement and the mixing capability between gas and particles. The gas velocity which the voids are initially observed in the bed is called the minimum bubbling velocity ( $u_{mb}$ ). The minimum bubbling velocity relies on particle size, density, and void fraction to mention some of them. Small bubbles are ideal because they make the gas move more uniformly throughout the bed, and results in particles to become more distributed in the fluid stream. But practically, the bubbles tend to coalesce and grow as they travel the bed upwards. [9]-[13]

Minimum fluidization velocity ( $u_{mf}$ ), which is an important parameter, is the velocity at which the bed material starts to have the same characteristics as a high viscous liquid. There are derived a variety of theoretical models to calculate minimum fluidization velocity. One of the most known theoretical models to predict minimum fluidization velocity is derived from the buoyancy-equals-drag balance, including the Ergun equation at low Reynolds numbers. This model is shown in equation (2.1). [9][10][13][14]

$$u_{mf} = \frac{d_p^2 \Delta\rho g}{150 \mu_g} * \frac{\Phi^2 \epsilon_{mf}^3}{1 - \epsilon_{mf}} \quad (2.1)$$

Where the  $\Phi$  is the sphericity of the bed material,  $\epsilon_{mf}$  is the void fraction at minimum fluidization velocity,  $d_p$  is the particle diameter,  $g$  is the gravitational acceleration,  $\Delta\rho$  is the difference in density between gas ( $\rho_g$ ) and particle ( $\rho_p$ ), and  $\mu_g$  is the gas viscosity. Wen and Yu have derived an approximate relation for equation (2.1) when the Reynold number is less than 20, as shown in equation (2.2). The relation is shown in equation (2.3). [9][10][13][14]

$$Re_{mf} = \frac{\rho_g u_{mf} d_p}{\mu_g} < 20 \quad (2.2)$$

$$\frac{\Phi_S^2 \varepsilon_{mf}^3}{1 - \varepsilon_{mf}} \cong \frac{1}{11} \quad (2.3)$$

With the relation shown in equation (2.3) implemented in equation (2.1), the finished result is as shown in equation (2.4).

$$u_{mf} = \frac{d_p^2 (\rho_p - \rho_g) g}{1650 \mu_g} \quad (2.4)$$

From equation (2.4), it is shown that the minimum fluidization velocity is dependent on particle diameter, gas viscosity, fluid density, and solid density. [9][10][13][14]

Equation (2.4) shows the theoretical approach to find the minimum fluidization velocity. The experimental approach to finding the minimum fluidization velocity is made by plotting the data with the pressure gradient vs. superficial velocity. The experimental approach is illustrated in Figure 2.3. [15]

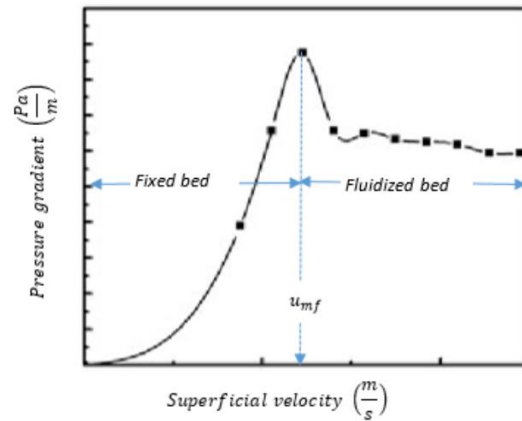


Figure 2.3: Graphical localization of minimum fluidization velocity in a pressure gradient vs. velocity plot. [15]

Figure 2.3 shows an ordinary pressure gradient vs. superficial velocity profile. When the pressure gradient is at its maximum, that is when the bed shift from a fixed bed to a fluidized bed. That means that the velocity at the maximum pressure gradient is the minimum fluidization velocity. [15]

After the bed is fluidized, the overall pressure gradient in the bed should have become smaller. Figure 2.4 illustrates the changes in the minimum fluidization profile after the bed is fluidized. [13]

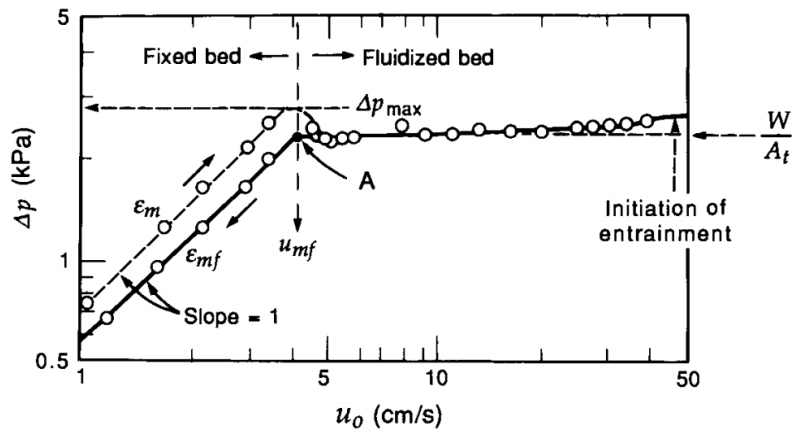


Figure 2.4: Ideal textbook behavior in a bed with uniformly sized sand represented in a pressure drop ( $\Delta p$ ) vs. superficial velocity ( $u_o$ ) plot. [13]

From Figure 2.4,  $\Delta p_{max}$  is the maximum pressure drop and  $\epsilon_m$  is the void when the bed has not been fluidized. After the bed has been fluidized, the void in-between the particles is higher than before fluidization. An increase in the void makes it easier for the fluid to travel between the particles, making the pressure drop over the bed smaller. This fluidized void ( $\epsilon_{mf}$ ) however is very sensitive, a little vibration or external interference may revert the  $\epsilon_{mf}$  back to  $\epsilon_m$ . When the void is back to its initial value after being fluidized, the maximum pressure drop must be reached again before the bed becomes fluidized. [13]

### 2.3 Principle of Gasification Reactions

The char created through pyrolysis of biomass is often composed of hydrocarbons and not only pure carbon. The number of hydrocarbons is of a certain amount and includes elements as hydrogen and oxygen. The characteristics of char made from biomass are it being more porous and reactive than coke made from carbonized coal. The char from biomass has a different behavior than chars from coal, lignite, or peat. The char from biomass becomes more reactive with conversion, while char from either coal, lignite or peat decreases in reactivity as its converse or as time goes. The difference in reactivity is mainly due to the difference in the size of the pores and porosity. The pores in char from biomass has a width of 20-30 $\mu\text{m}$ , while the char from coal has a width of roughly 0.0005  $\mu\text{m}$ . The porosity between char from biomass and coal is in the range of 40-50% and 2-18%, respectively. The opposite trend is shown in Figure 2.5, where the gasification of peat is represented with purple data points, and hardwood is with blue data points. [5][7]

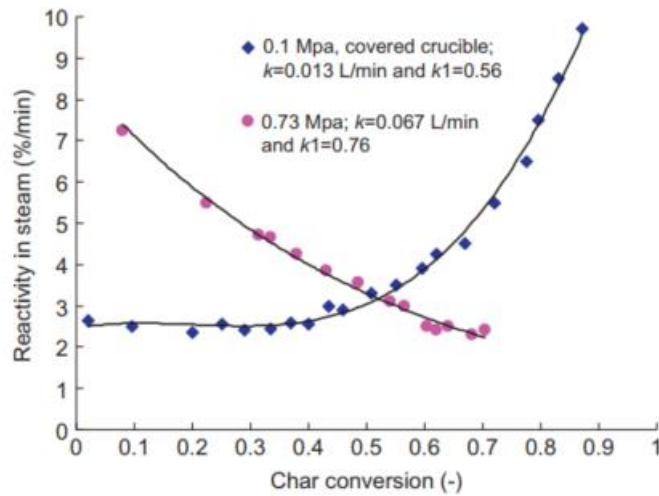


Figure 2.5: Peat vs. hardwood under gasification in steam compared in a conversion diagram. [5]

A big part of biomass gasification is the several chemical reactions between the gasifying medium and the char. Some examples of these reactions are shown in equation (R 2.2) – (R 2.5), where solid carbon, hydrogen, carbon dioxide, hydrogen, steam, and methane are present. [5][7]



As seen from equation (R 2.2) – (R 2.5), these reactions are not balanced, but only represents an example of the possible outcome when reacting char with gasifying mediums. The solid carbon is reacting with different gasifying mediums and converts into low-molecular-weight gases like carbon monoxide and hydrogen, which is shown balanced in Table 2.3. [5][7]

Table 2.3 shows some of the essential chemical reactions happening under gasification with the heat of reaction at 25 °C. [5]

Table 2.3: Chemical reactions in a gasification process represented with the heat of reaction at 25°C. [5]

Reaction Type	Chemical Reaction Equations	
<b>Carbon Reactions</b>		
Boudouard	$C + CO_2 \leftrightarrow 2CO + 172 \text{ kJ/mol}$	(R 2.6)
Water-gas or steam	$C + H_2O \leftrightarrow CO + H_2 + 131 \text{ kJ/mol}$	(R 2.7)
Hydrogasification	$C + 2H_2 \leftrightarrow CH_4 - 74.8 \text{ kJ/mol}$	(R 2.8)
	$C + 0.5O_2 \leftrightarrow CO - 111 \text{ kJ/mol}$	(R 2.9)
<b>Oxidation Reaction</b>		
	$C + O_2 \rightarrow CO_2 - 394 \text{ kJ/mol}$	(R 2.10)
	$CO + 0.5O_2 \rightarrow CO_2 - 284 \text{ kJ/mol}$	(R 2.11)
	$CH_4 + 2O_2 \leftrightarrow CO_2 + 2H_2O - 803 \text{ kJ/mol}$	(R 2.12)
	$H_2 + 0.5O_2 \rightarrow H_2O - 242 \text{ kJ/mol}$	(R 2.13)
<b>Shift Reaction</b>		
	$CO + H_2O \leftrightarrow CO_2 + H_2 - 42.2 \text{ kJ/mol}$	(R 2.14)
<b>Methanation Reaction</b>		
	$2CO + 2H_2 \rightarrow CH_4 + CO_2 - 247 \text{ kJ/mol}$	(R 2.15)
	$CO + 3H_2 \leftrightarrow CH_4 + H_2O - 206 \text{ kJ/mol}$	(R 2.16)
	$CO_2 + 4H_2 \rightarrow CH_4 + 2H_2O - 165 \text{ kJ/mol}$	(R 2.17)
<b>Steam-Reforming Reaction</b>		
	$CH_4 + H_2O \leftrightarrow CO + 3H_2 + 206 \text{ kJ/mol}$	(R 2.18)
	$CH_4 + 0.5O_2 \rightarrow CO + 2H_2 - 36 \text{ kJ/mol}$	(R 2.19)

The gasification process is an endothermic process in nature, but there are some exothermic reactions as well. Reaction (R 2.8), (R 2.9), and (R 2.10) from Table 2.3 are exothermic reactions, while reaction (R 2.6), and (R 2.7) are endothermic reactions. [5]



## 2 Biomass Gasification

The reaction rate is controlled by the reactivity and the potential of reaction with the gasifying medium. The reactivity between the mediums can be ranked as, where the most reactive is oxygen: [5][7]

1. Oxygen
2. Steam
3. Carbon Dioxide
4. Hydrogen

The difference in reaction rate is also illustrated in Table 2.4, with equation (R 2.6) – (R 2.9) from Table 2.3 listed from fastest to slowest. [5]

Table 2.4: Gasifying mediums reaction rate represented as an order of magnitude.[5]

Type of reaction	Reaction	Order of magnitude slower
Eq(R 2.9) Char-Oxygen	$C + 0.5O_2 \leftrightarrow CO$	Reference/Fastest
Eq(R 2.7) Char-Steam	$C + H_2O \leftrightarrow CO + H_2$	Three to five
Eq(R 2.6) Char-Carbon Dioxide	$C + CO_2 \leftrightarrow 2CO$	Six to seven
Eq(R 2.8) Char-Hydrogen	$C + 2H_2 \leftrightarrow CH_4$	Slowest/below seven

### 2.4 Agglomeration in a Bubbling Fluidized Bed

After the char has been gasified, there are only inorganic solid residues left in the reactor. These inorganic solid residues are called ash, and primarily contains iron, calcium, and aluminum, but also small amounts of potassium, sodium, titanium, and magnesium. The amount of ash from biomass is usually minimal. However, even a small amount of ash can play a significant role in biomass utilization, especially if it contains alkali metals, these alkali metals can be potassium or chlorine. Components such as grasses, demolition wood, and straw have a high potential to create agglomeration, fouling, and corrosion in a gasifier. [5]

The operating temperature for biomass fluidized bed gasifiers usually is around 900 °C. The temperature at which the biomass ash is melting varies. The melting temperature is affected by the type of biomass used, and the composition of the biomass ash. An example of the difference in biomass ash melting temperature is shown in Table 2.5, where there are three different biomasses with three different ash melting temperatures. The composition of the biomass is not shown. [5][10]

Table 2.5: Ash melting temperature for three different biomasses. [10]

Type of Biomass	Biomass Ash Melting Temperature [°C]
Spruce Wood	1170
Miscanthus Giganteus	940
Wheat Straw	915

## 2 Biomass Gasification

When the ash melts or partial melts, the inorganic alkali from the melted ash may under certain conditions create a sticky component, which functions as an adhere between the ash components and the silica in the sand. With this adhesive function in the bed, a bigger entity than the existing bed particles may be formed. This bigger entity, consisting of both the bed material and the components from melted ash, is called an agglomerate. Figure 2.6 shows multiple agglomerates which are created by melted biomass ash and sand particles. [5][15][16]



Figure 2.6: Agglomerates from fluidized bed biomass gasification.

The agglomerates are shown to be of various sizes and shapes, thus making them harder to fluidize sufficiently like the bed material. An agglomerated bed creates instability in the bubble frequency and fluid channeling. Agglomeration can also lead to zones in the fluidized bed where it may defluidize. In the end, the fluidized bed can suddenly and completely defluidize. The bubble frequency and defluidized zones are illustrated in Figure 2.7. From experimental studies [15], agglomerates are approximated to have a size that varies between 2 cm to 8 cm with a density of  $1506 \text{ kg/m}^3$ . [15]-[17]

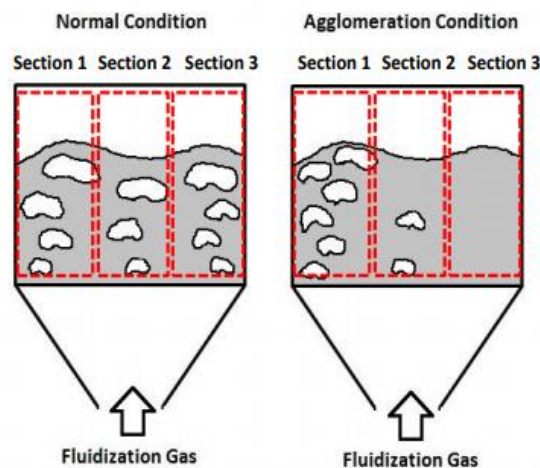


Figure 2.7: Fluidized bed bubbling frequency, both with and without agglomerates. [18]

## 2 Biomass Gasification

Depending on where the agglomeration is located initially in the bed, the  $\Delta p_{max}$  may increase or decrease. The  $\Delta p_{max}$  is lower when the agglomeration is located at the bottom and higher when located at the top. Figure 2.8 and Figure 2.9, shows experimental data where agglomerates have a different location in the bed. In an agglomerated bed, the overall pressure drop is lower compared to the normal fluidized bed. The overall minimum fluidization velocity increases with agglomeration. The minimum fluidization velocity and the  $\Delta p_{max}$  is at the highest when agglomeration is located at the top of the bed. [15][16]

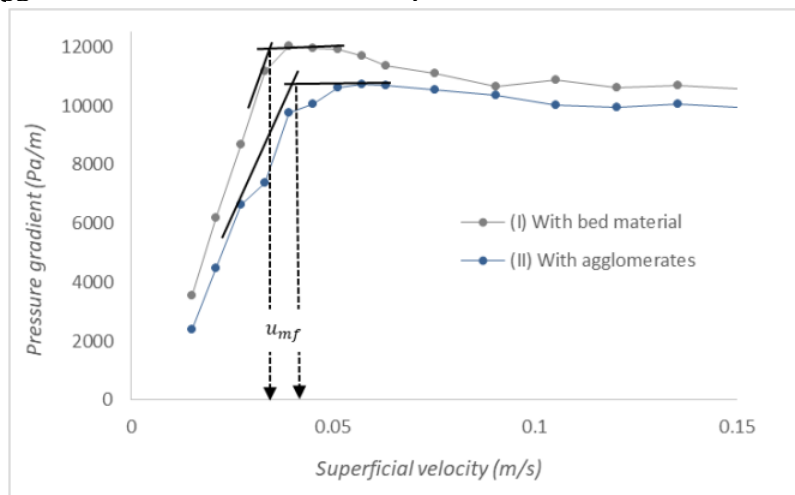


Figure 2.8: BFB experiment with no agglomerates (I) and with agglomerates at the bottom of the bed (II). [15]

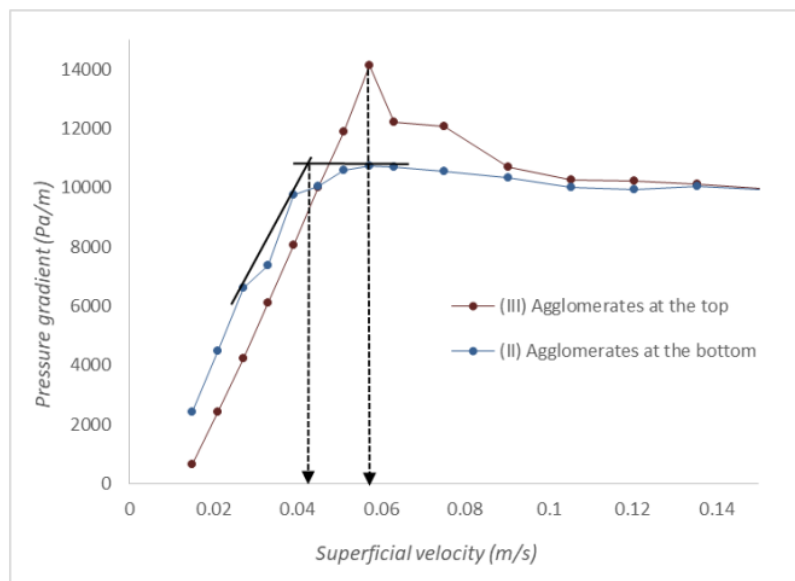


Figure 2.9: BFB experiment with agglomerates at the bottom (II) and top (III) of the bed. [15]

## 3 Scaling of Bubbling Fluidized Bed Reactor

This chapter includes the background of why scaling is used and how to correctly scale from lab size to a pilot size BFB reactor.

### 3.1 Glicksman's Rule of Scaling

The operation conditions in fluidized bed reactors are usually with high temperatures. High temperatures provide difficulties when investigating the fluid dynamics in bed. It is also considered inconvenient to stop a running reactor too conduct experiments, measurements, and other forms of research purposes, especially when the reactor requires to operate continuously. [9]

With scaling, there is the possibility to design, investigate, and measure the reactor while it is in lab size, then scale it up to a pilot or industrial-sized with the same fluid dynamic similarities. To receive the same fluid dynamic similarities between the two scaled reactors, properly developed scaling rules must be used. [9]

Glicksman proposed to use a derived set of dimensionless parameters build upon the governing conservation equation of particles and fluid. [9]

Equation (3.1), shows the full set of Glicksman's independent dimensionless parameters.

$$\frac{u_0^2}{gL}, \frac{\rho_p}{\rho_g}, \frac{\rho_g u_0 d_p}{\mu_g}, \frac{L_1}{L_2}, \frac{L}{d_p}, \Phi, PSD \quad (3.1)$$

From equation (3.1),  $u_0$  is the superficial velocity,  $L$  is a chosen length dimension,  $L_1$  and  $L_2$  is the characteristic length dimension for pilot-scale and lab-scale respectably. The ratio  $u_0^2 / gL$  is also known as the Froude number. [19]-[21]

According to Glicksman, the beds have fluid dynamic similarities if the dimensionless parameters from equation (3.1) are identical to each other. But to have all the dimensionless parameters to be identical to each other is difficult to do in practice. Glicksman took this into account and simplified the set of parameters from equation (3.1) to become as shown in equation (3.2). The Reynolds number is replaced with the ratio of superficial gas velocity  $u_0$  over minimum fluidization velocity  $u_{mf}$ . [19]-[21]

$$\frac{u_0^2}{gL}, \frac{\rho_p}{\rho_g}, \frac{u_0}{u_{mf}}, \frac{L_1}{L_2}, \frac{L}{d_p}, \Phi, PSD \quad (3.2)$$

The parameters from equation (3.2) are affected by two flow conditions. These are when the fluid-particle drag is dominated by inertia forces and viscous forces. The inertial dominated flow is when there are big particles at high velocity. The Inertial limit is at Reynolds number equal to or higher than 400. [19]-[21]

Similarly, a viscous dominated flow is when there are small particles at low velocity. At these flow conditions, the fluids inertial forces are insignificant. The viscous dominated flow limit is when the Reynolds number is lower than 4. [19]-[21]

### 3 Scaling of Bubbling Fluidized Bed Reactor

When the Reynolds number is 4 or less, the density of the fluid is negligible and thus omitted. With the new condition, the parameters from equation (3.2) are then simplified to become as shown in equation (3.3). The set of equations is known as Glicksman's viscous limit set of dimensionless parameters. [19]-[21]

$$\frac{u_0^2}{gL}, \frac{u_0}{u_{mf}}, \frac{L_1}{L_2}, \frac{L}{d_p}, \Phi, PSD \quad (3.3)$$

## 4 Experimental Work

This chapter covers experiments conducted on two different lab sized models of a BFB. Data gathered from these two experimental set-ups are used for comparing and verifying the simulated data. The difference between the two columns is that one is configured to include gasification while the other does not. The columns are named BFB-gasifier and Cold-BFB, respectively. There are conducted five experimental cases. Three of these cases are for Cold-BFB, and the two last cases are for BFB-gasifier.

Both the experimental models use sand as bed material, but the sand may vary in size and size distribution. The sand size and distribution for both the experiments are found through sieve analysis.

Gasification experiments were performed with two different mass flow rates of air. For each of the mass flow rates, the temperature and the pressure were noted. There was done three temperature- and pressure- notations with a 10-minute break between them.

### 4.1 Cold-BFB

The Cold-BFB consists of a transparent cylindric tube. The Cold-BFB is open to the atmosphere at the top and with a distributor plate at the bottom. The height and diameter of the cylinder are 140 cm and 8.4 cm, respectively. There are Pressure transducers installed along the BFB, and the distance between the transducers is 10 cm. The model is shown in Figure 4.1. [22]

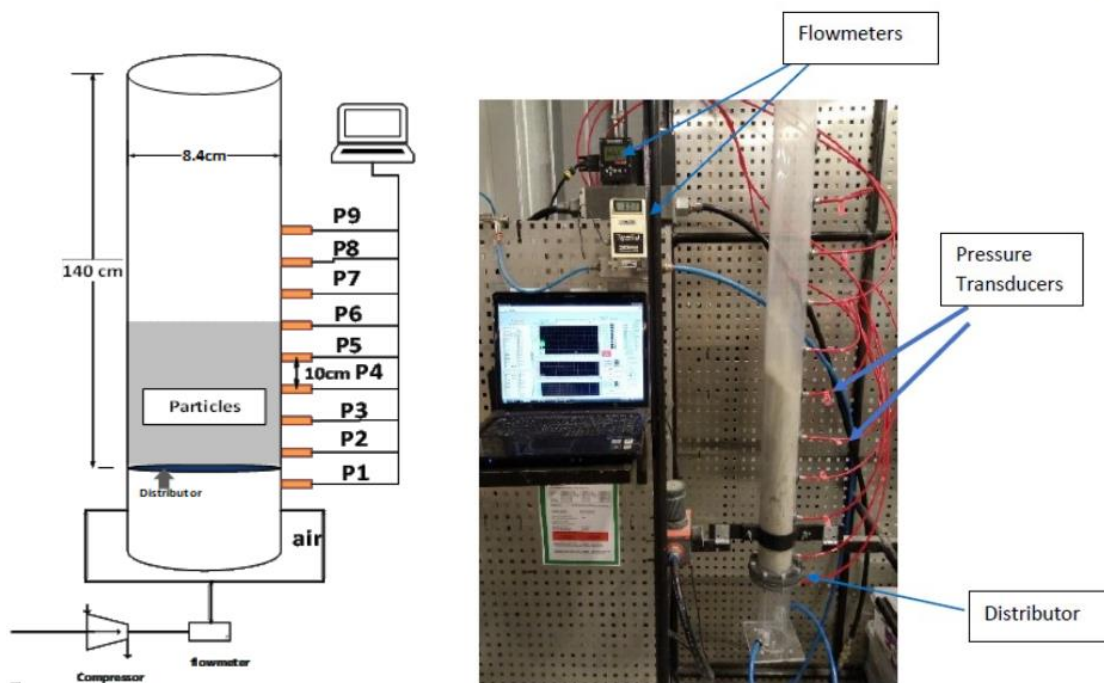


Figure 4.1: Experiment, Cold-BFB: the layout, set up, and dimensions for the column. [22]

## 4 Experimental Work

The distributor plate is located between the pressure transducers  $P_1$  and  $P_2$ . The distance from the distributor plate to  $P_2$  is 3.5 cm. The air was controlled and measured using a flowmeter. The flowmeter showed the measurement in normal liter per minute (NLPM or NI/min). The pressure transducers were read and converted by the software LabVIEW, which also writes the results in a text file. [22]

### 4.1.1 Sieve Analysis

The sieves used in the analysis are standard laboratory/test sieves, as shown in Figure 4.2.



Figure 4.2: Laboratory sieves. [23]

These sieves were used with a sieve shaker, as shown in Figure 4.3, to increase efficiency when performing a size distribution analysis.



Figure 4.3: Sieve shaker. [24]

The sand particles used as bed material were in a size range of 300-700  $\mu\text{m}$ . The sieve sizes used in this experiment is 355  $\mu\text{m}$ , 425  $\mu\text{m}$ , 500  $\mu\text{m}$ , and 600  $\mu\text{m}$ . The sieve analysis can be found in Appendix B. The mean particle size can be calculated using equation (4.1) and gives a value of 535  $\mu\text{m}$ .

$$\bar{d}_p = \frac{\sum WF}{\sum \frac{WF}{d_p}} \quad (4.1)$$

### 4.1.2 Bed Parameters Descriptions

Both the height and the diameter of the Cold-BFB is known from Figure 4.1. The bed height was found by using the aspect ratio, as shown in equation (4.2). The aspect ratio was chosen to be 2.5, which corresponds to neither a shallow bed nor a deep bed, and provides a height that completely covers sensors P<sub>2</sub> and P<sub>3</sub>. [25]

$$\text{Aspect Ratio} = 2.5 = \frac{h}{D} \quad (4.2)$$

$h$  is the height of the bed, and  $D$  is the diameter of the Cold-BFB. The bulk density is found from:

$$\rho_{bulk} = \frac{m_{bed}}{V_{bed}} \quad (4.3)$$

$\rho_{bed}$  is the bulk density of the bed. The bulk density is being used to determine the particle volume fraction of the bed. The particle volume fraction is calculated using equation (4.4).

$$\theta_p = \frac{\rho_{bed}}{\rho_p} \quad (4.4)$$

Where  $\theta_p$  is the particle volume fraction, and  $\rho_p$  is the particle density. Sand is used as bed material and has a density of 2650 kg/m<sup>3</sup>. The parameters can be found in Table 4.1.

Table 4.1: Experiment, Cold-BFB: calculated bed parameters.

Symbol	Result	Unit
$h$	0.21	$m$
$V$	1.16e-3	$m^3$
$\rho_{bulk}$	1407	$\frac{kg}{m^3}$
$\theta_p$	0.53	—

All of the data from Table 4.1 is based on the theoretically calculated bed height. The volume was used to measure the amount of sand needed for the bed. After filling sand into the BFB, the bed height was measured and found to be less than the calculated height. The cause is thought to be that when the sand was filled into the column, the sand was poured from the top, making it travel freely in roughly 1.4 m. The free fall of 1.4 m may have created a more packed bed than anticipated. The newly calculated data with the new measured height can be seen in Table 4.2.



Table 4.2: Experiment, Cold-BFB: corrected bed parameters.

Symbol	Result	Unit
$h$	0.196	$m$
$V$	1.09e-3	$m^3$
$\rho_{bulk}$	1507	$\frac{kg}{m^3}$
$\theta_p$	0.57	—

### 4.1.3 Experimental Results

The airflow was controlled by a flowmeter, and the unit was in  $Nl/min$ . The airflow was adjusted to run from 25  $Nl/min$  to 85  $Nl/min$  with a 5  $Nl/min$  increment every 120 seconds. The data writing starts 60 seconds after an incrementation change, thus providing the bed 60 seconds to stabilize before the data is noted. The airflow is converted to  $m/s$ , as shown in Table 4.3. The data is displayed with a pressure gradient vs. superficial velocity, as shown in Figure 4.4.

Table 4.3: Experiment, Cold-BFB: volumetric flow rate converted to linear velocity.

$\frac{Nl}{min}$	$\frac{m}{s}$	$\frac{Nl}{min}$	$\frac{m}{s}$
25	0.08	60	0.18
30	0.09	65	0.20
35	0.11	70	0.21
40	0.12	75	0.23
45	0.14	80	0.24
50	0.15	85	0.26
55	0.17		

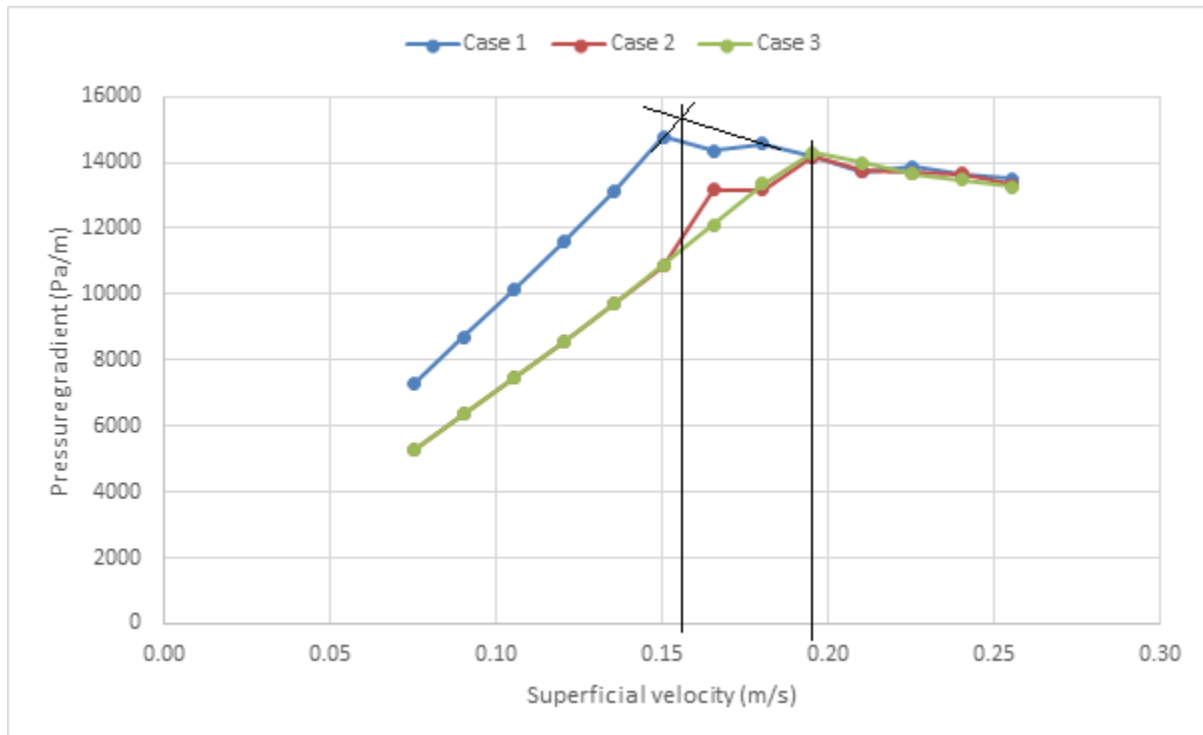


Figure 4.4: Experiment, Cold-BFB: experimental data displayed in a pressure gradient vs. superficial velocity plot with the locations of minimum fluidization velocities.

The figure shows three cases, Case 1 (blue), 2 (red), and 3 (green). The blue line represents the first run, where the sand has not been fluidized. The red and green line is when the fluidized bed is going in an incrementing way down to its initial velocity of 0.08 m/s from fluidized state and up again to 0.26 m/s, respectively. The minimum fluidization velocity is 0.16 m/s and 0.19 m/s for the non-fluidized void and fluidized void, respectively. The experimental result does deviate compared to Figure 2.4, where the minimum fluidization velocity is the same for both the non-fluidized void and fluidized void. The deviation may be because the literature is using one uniformly sized particle as bed material while in the experiment, a particle size distribution is used. Since the bed contains a wide range of particle sizes, the particles in the bed may segregate when fluidized. The smaller particles may be carried to the top of the bed while the bigger particles stay stationary. If segregation occurs, then the transducers may only have large particles between them, while the smaller particles segregate. If there are only big particles between the transducers, then a higher minimum fluidization velocity could occur. The minimum fluidization velocity is proportional to the particle diameter squared. [13]

Case 1 from Figure 4.4 is used for further comparison and is referred to as “Experiment: Cold-BFB” in the figures.

## 4.2 BFB-Gasifier

The BFB-gasifier is a cylindrical column made of stainless steel. It has three electrical heating elements which are installed externally. They are capable of heating the reactor to 1000 °C. The gasifier is insulated with refractory material on the inside, and a 200 mm thick fiberglass layer on the outside to minimize the heat losses. The BFB-gasifier is shown in Figure 4.5. [26]



Figure 4.5: Experiment, BFB-gasifier: set up viewed from the right side.

From the left side in Figure 4.5 is the furnace, which is used to burn the product gas, then the BFB-gasifier in the center, and the biomass feeder at the far right. Figure 4.6 shows the BFB-gasifier from another perspective.



Figure 4.6: Experiment, BFB-gasifier: set up viewed from the left side.

From Figure 4.6, the BFB-gasifiers can be seen in the center. The rods pointing out are connected to sensors that measure the temperature and pressure at different locations along

## 4 Experimental Work

with the height of the fluidized bed. Figure 4.7 illustrates the position of the sensors, the diameter of the bed, and the feeding position.

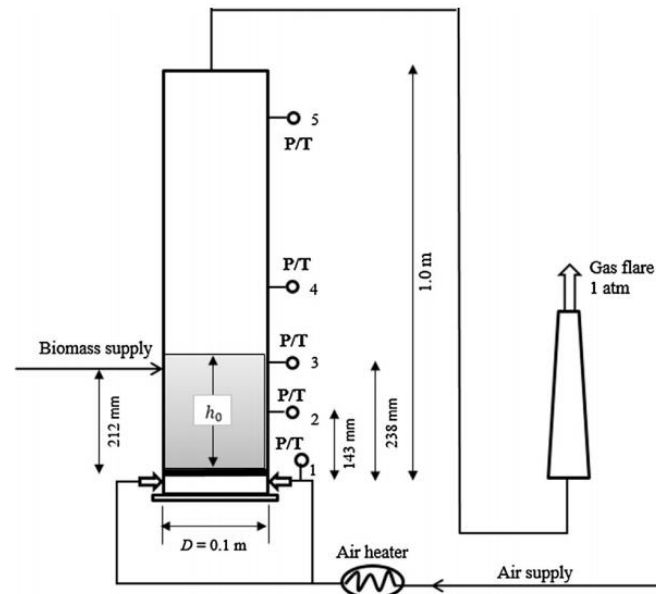


Figure 4.7: Experiment, BFB-gasifier: layout and dimensions. [26]

The column is 0.1 m in diameter and 1 m in height. The sensors are located, as shown in Figure 4.7, where the distance between sensor  $P_3$  and  $P_2$  are 0.095 m. The pressure and temperature data were recorded by a provided computer program.

Sand with a mean particle diameter of 367  $\mu\text{m}$  was used in the experiments. The data from the sieving analysis are presented in Appendix B.

### 4.2.1 Bed Parameters Descriptions

The mass flow rates of air used in the gasification experiment are 1.5 kg/hr and 2.0 kg/hr, with an averaged temperature of 733  $^{\circ}\text{C}$  and 735  $^{\circ}\text{C}$ , respectively. Since these temperatures vary with 2  $^{\circ}\text{C}$ , it is chosen to only use the highest temperature for further calculations. The velocities converted from the gas flow rates with adequate parameters are shown in Table 4.4.

## 4 Experimental Work

Table 4.4: Experiment, BFB-gasifier: parameters for the mass flow rate to linear velocity conversion.

Parameter	Case 4	Case 5
$\dot{m}_{air}$	$1.5 \frac{kg}{hr}$	$2.0 \frac{kg}{hr}$
$\rho_{Air @ 735^{\circ}C}$	$0.35 \frac{kg}{m^3}$	$0.35 \frac{kg}{m^3}$
$A$	$7.85e-3m^2$	$7.85e-3m^2$
$u_{air}$	$0.15 \frac{m}{s}$	$0.20 \frac{m}{s}$

When preparing the bed material, weight and volume are measured. The weight and volume were measured to be 2.331 kg and 1.6 l with sand, respectively. The height, volume, bulk density, and particle volume fraction for the bed can be found in Table 4.5

Table 4.5: Experiment, BFB-gasifier: calculated bed parameters.

Parameter	Value	Unit
$h$	0.20	$m$
$V$	1.6e-3	$m^3$
$\rho_{bulk}$	1457	$\frac{kg}{m^3}$
$\theta_p$	0.55	—

### 4.2.2 Experimental Results

A plot of the pressure gradient vs. superficial gas velocity is presented in Figure 4.8. The figure shows two data points that represent the two mass flow rates of air used in the experiment. Case 4 has an average pressure gradient of 10001 Pa/m at a gas velocity of 0.15m/s, while Case 5 has an average pressure gradient of 12469 Pa/m at a gas velocity of 0.20 m/s.

## 4 Experimental Work

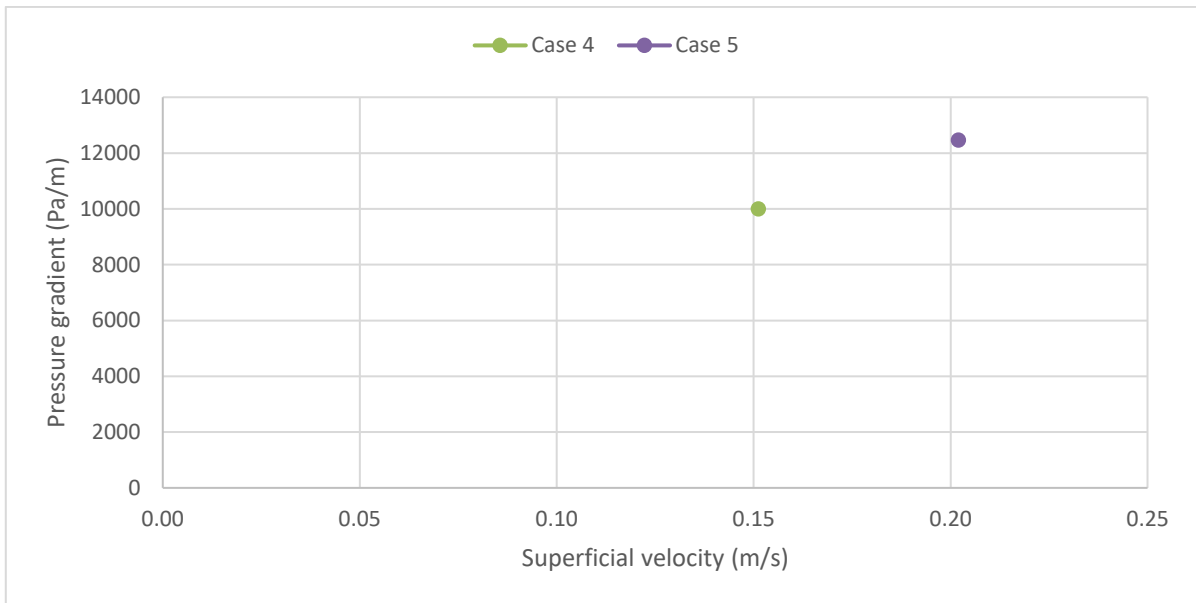


Figure 4.8: Experiment, BFB-gasifier: experimental results plotted in a pressure gradient (Pa/m) vs. superficial velocity (m/s).

To check if the bed was fluidized during the experimental tests. Equation (2.4) is used to calculate the minimum fluidization velocity at 735 °C. The minimum fluidization velocity is found to be 0.051 m/s for this experiment, which indicates that the bed is in the fluidized region for both the gas velocities.

## 5 CPFD Model Development

To simulate the fluidized bed and the formation of agglomerates in the fluidized beds, a computational particle fluid dynamic (CPFD) software was used. The simulation software Barracuda Virtual Reactor (VR) version 17.4.1 specializes in particle movements and behavior with chemistry. The software uses the numerical method Multiphase Particle-In-Cell (MP-PIC). MP-PIC is an approach to the Discrete Parcel Method (DPM). DPM is a method where a group of particles are identified and tracked instead of individual particles. Each group is assumed to have the same properties and is thus represented by one computational particle. [16][27][28]

The goal is to make a model that would predict the experimental pressure gradient profile and minimum fluidization velocity from the BFB-gasifier. Then utilize that model to simulate the flow behavior when agglomerates are present in a bubbling fluidized bed.

### 5.1 Computational Fluid Dynamic

Computational fluid dynamic has been used for over 50 years and was invented at the Los Alamos Laboratory in the 1960s. CFD is used to simulate and solve real-world fluid behavior and flow events, and this is all from processes where fluid behavior in pipe or tank is important to air behavior over a vehicle. CFD uses computational power to solve advanced mathematical expressions and physical movements of fluids, where fluids are mainly liquids and gases. CFD was for a long time also used to model and predict the behavior and movements of particles. However, since particles are solids, it did provide limited functions and not completely accurate solutions. This limited function and not completely accurate in prediction is the reason that CPFD software was developed. CPFD models predict the behavior of particles in various types of equipment. [29]

## 5.2 Barracuda

On the left side of the interface, there is a window named “Project Tree”. The project tree is the window that contains all the different features, e.g., set-up grid, global settings, base materials, initial conditions, boundary conditions. The most relevant and influential of these features are addressed further in this chapter. [28]

### 5.2.1 Global Setting and Base Material

The global settings address the parameters that affect the entire model; these can be such as gravity, temperature, and when the chemistry should be activated. As a global setting for all the simulations conducted, gravity was set to be  $[0, 0, -9.8] \text{ m/s}^2$  as default value. This value tells the software that there is no gravity in the x- and y- direction, but a normal gravity acceleration in the z-direction. The temperature is default at an isothermal flow of 300 K. The chemistry settings are left at the default setting. [28]

The base material is where the material used in the model is defined. The material is specified as either gas, liquid, or solid, and there is also the possibility to specify the physical properties for the material, e.g., density, incompressible, mole average, or mass average. [28]

The materials chosen initially are sand and air. The sand has a density of  $2650 \text{ kg/m}^3$ , and the default properties are used for air. Both the components were chosen to be compressible. [28]

### 5.2.2 Particle Description

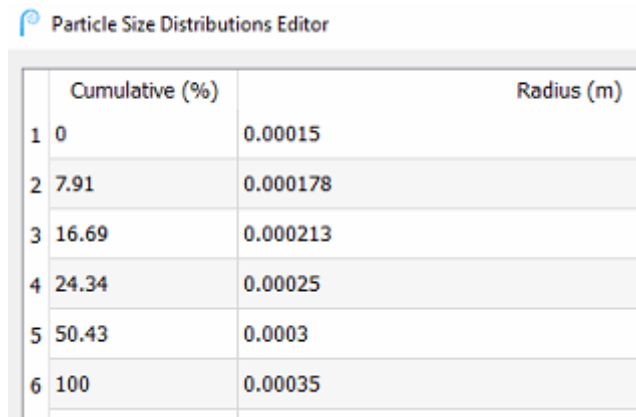
The particle section of the project tree is where the user can enter the global settings for the particle and include the species that the bed particle is composed of. The global particle settings used are: [28]

- Close Pack Volume Fraction: 0.6
  - Maximum momentum redirection from collision: 40%
  - Normal to wall retention: 0.85
  - Tangent to wall retention: 0.85
  - Diffuse Bounce: 5

The close pack volume fraction (CPVF) is the setting that tells the software the maximum ratio between the fluid and particles, and it is typical around 0.56 to 0.64. The maximum momentum redirection from collision is the percentage of the energy lost when colliding with the particle. Both normal- and tangent- to wall retention is the momentum after collision with the wall. If both were 1, then the collision would have been 100 % elastic. Diffuse bounce is a scatter function that affects the values chosen for normal- and tangent- to wall retention. If the function is left at zero, it can make the simulation very static, but with diffuse bounce equal to 5, it is more dynamic. [28]

Under particle settings, there is the possibility to specify for each particle and its physical properties. As there is only sand used in the initial runs, there are no other species needed to address at this point. The sand size distribution is made in a table, as shown in Figure 5.1, these values are from the Cold-BFB sieve analysis, but converted to a cumulative percentage. [28]



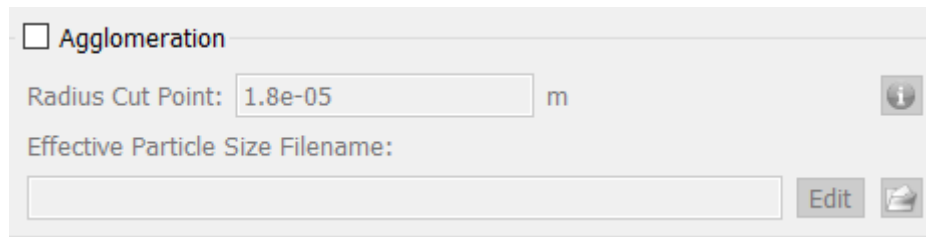


	Cumulative (%)	Radius (m)
1	0	0.00015
2	7.91	0.000178
3	16.69	0.000213
4	24.34	0.00025
5	50.43	0.0003
6	100	0.00035

Figure 5.1: Parameter, Cold-BFB model: PSD sheet.

The sphericity for the sand is chosen to be 0.68 based on visual and tactile data. The emissivity is set to be the default value, which is 1. [28]

The specifying particle species section also has the possibility to create agglomerates with the particle. The agglomeration setting makes the bed particles imitating itself to become larger particles than what it originally is. In short, the same amount of bed particles are there, but some of them imitate to be bigger than the rest. Figure 5.2 shows the agglomeration function in Barracuda. [28]



Agglomeration

Radius Cut Point:  m

Effective Particle Size Filename:

Figure 5.2: Barracuda: built-in agglomeration function.

The different drag models are tested later in the chapter. There is no chemical reaction performed during the simulations, so volatiles are not specified. [28]

### 5.2.3 Set-up Grid

The set-up grid section is where the user can import, view, and create a grid for the geometry. [28]

The geometry is created using software that handles CAD geometries; this can be software such as AutoCAD or SolidWorks. After the geometry is created, the geometry is saved as a .stl file. Barracuda recognizes .stl files as geometry, and thus the file can be imported into the software. Two geometries were created initially, the geometry for the Cold-BFB and the BFB-gasifier. The BFB-gasifier is addressed in Chapter 5.4, and the Cold-BFB geometry follows the same cylindrical dimensions, as explained in Chapter 4.1, which is 0.084 m in diameter and 1.4 m in height. The CAD geometry for Cold-BFB is shown in Figure 5.3. [28]



Figure 5.3: Cold-BFB model: CAD geometry.

The grid is straightforward to make in Barracuda, as it makes most of the adaptation for the user. The software provides a tool that can automatically uniformly distribute the cells and test the grid if it has any regions that are non-uniformly. There is also a possibility to create sections, and then choose different grid resolution for each section in the geometry. Barracuda uses a three-dimensional cartesian coordinate system for the grid. [28]

The default grid resolution was set to be 12000 total cells; this resulted in a uniformly distributed grid of 9536 cells for the Cold-BFB CAD geometry. As shown in Figure 5.4, there are not any non-uniformly regions in the grid. The grid resolutions do not vary in any of the geometries; thus, the grid check is not used in further simulations.

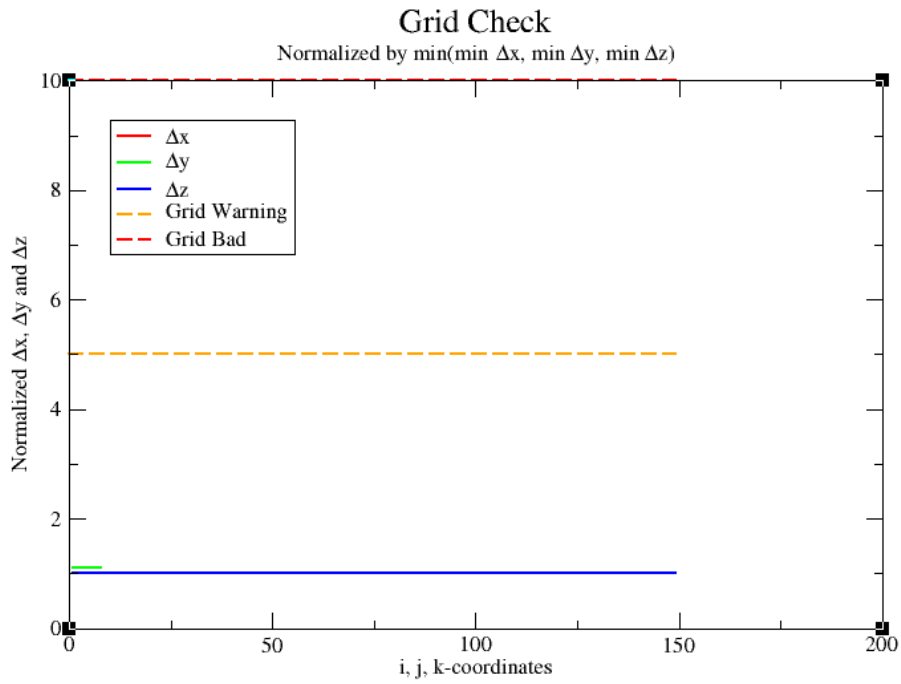


Figure 5.4: Cold-BFB: The provided grid check tool from Barracuda.

The uniform cell distribution represented in a 2-D geometry can be seen in Figure 5.5, and Figure 5.6 shows a 3-D representation of the grid.

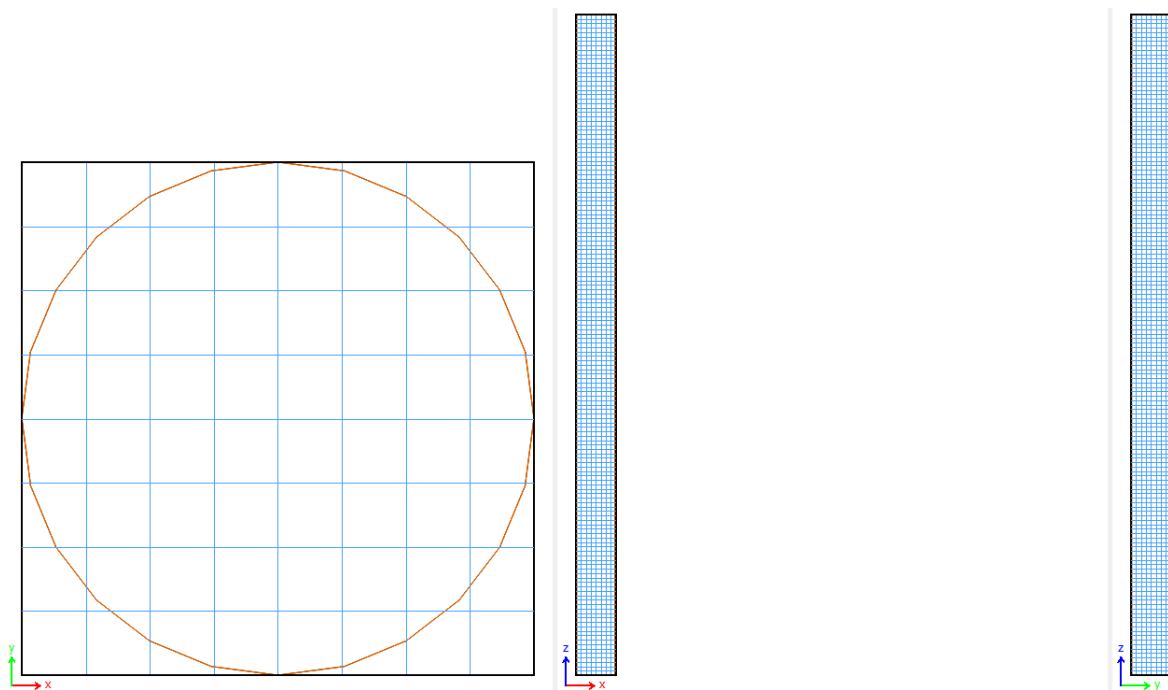


Figure 5.5: Cold-BFB: grid layout presented in 2-D.



Figure 5.6: Cold-BFB: grid layout presented in 3-D.

From Figure 5.5, the number of cells along the diameter is 8 cells. 8 cells in “physical” size is then  $8.4 \text{ cm}/8 = 1.05 \text{ cm}$ . The cells have a dimension of roughly 1cm in each direction as the cells are cubes. The physical size of the grid is crucial as the grid cells cannot be smaller than the size of the particles.

### 5.2.4 Initial Conditions

The initial conditions (IC) are where the user chooses the location, velocity, and pressure that the fluid and particles have. The IC for the fluid is air at 1 atm with no velocity. The air is also occupying the whole column.

IC for the particle is occupation from bottom to 0.196 m in the z-direction, and the particle volume fraction is 0.57. These values are based on the calculations and measurements done in chapter 4.1.1 and found in Table 4.2. The temperature is 300 K.

### 5.2.5 Boundary Conditions

The boundary conditions (BC) are used to specify the location of the inlet and outlet. The boundaries conditions employed in the current work are the pressure- and flow- BC, as illustrated in figure Figure 5.7. The pressure- and flow- BC is in color yellow and red, respectively. [28]



Figure 5.7: Cold-BFB: layout for the boundary conditions.

The pressure BC is set to be located at the top of the geometry. The pressure BC is specified to operate in the z-direction, to be open to the atmosphere, and no particles should exit the control volume. The fluid occupying at the pressure BC is specified to be air.

The flow BC is the red section on the bottom of the column. The flow BC is specified as air inlet flow. The flow profile through the flow BC is transient and changes with a specified time. Table 5.1 shows the initial flow chart based on the velocity profile from the Cold-BFB experiment in Table 4.3.

Table 5.1: Parameter, Cold-BFB model: Boundary condition, the initial flow chart.

<i>Time</i>	Velocity	<i>Time</i>	Velocity
[s]	$\left[\frac{m}{s}\right]$	[s]	$\left[\frac{m}{s}\right]$
0	0.08	35	0.18
5	0.09	40	0.20
10	0.11	45	0.21
15	0.12	50	0.23
20	0.14	55	0.24
25	0.15	60	0.26
30	0.17		

The time is the simulation time in seconds. Every velocity runs for five seconds each before it increases the velocity.

### 5.2.6 Numerics

The numerics section is where the user can tune the solver settings. The user can also adjust the turbulence model and its parameters. All of the settings in the numerics section are chosen to be at default. [28]

The turbulence and advection options are where the model and schemes are chosen. The default settings use Large Eddy Simulation (LES) as a turbulence model and partial donor cell as a numerical advection scheme. [28]

### 5.2.7 Time Controls

In time controls, the user can set the duration and timestep of the simulation. As a default, the timestep was set to be 0.001 seconds, and the duration was for 65 seconds. 65 seconds provides 5 seconds for the last velocity in Table 5.1 to have the same duration as the other velocities.

### 5.2.8 Data Outpoints and Post-run

The data outpoints section is where the user can specify the form that the data output should have. The user can also choose to have various data outpoints that read transient data, such as temperature, pressure, and particle temperature. These data outpoints works like sensors and makes it possible to plot the results after the simulation. The sensor type used is pressure, and the locations for the pressure sensors are as shown in Table 5.2. The post-run is where images and videos can be created from the outputted data.

## 5 CPFD Model Development

Table 5.2: Parameter, Cold-BFB model: pressure sensor coordinates.

Sensor number	Coordinates [x,y,z]
Pressure Sensor 1	[0.0423, 0.0423, 0.035]
Pressure Sensor 2	[0.0423, 0.0423, 0.135]

The pressure sensors  $P_1$  and  $P_2$  are at the same z-height as the transducers in the experimental Cold-BFB model. The location of the pressure sensors is shown in Figure 5.8. The sensors are the blue dots in the center of the geometry.



Figure 5.8: Cold-BFB: pressure sensor location in the geometry.

### 5.3 Cold-BFB Model

The initial parameter values used are described in Chapter 5.2.

#### 5.3.1 Testing of Various Drag Models

Five drag models from Barracuda's list were tested to see which one would fit the experimental results from Chapter 4.1.3 best. The selected drag models were chosen based on familiarity and the description that Barracuda provided on them. The result from the different drag models is compared to each other and then with the experimental data from Figure 4.4. The five chosen drag models were Wen-Yu, Ergun, WenYu-Ergun, Turton-Levenspiel, and Nonspherical-Haider-Levenspiel.

Due to simplicity and insufficient time, all parameters used in the drag models are at their default value given by Barracuda.

The calculated force, Reynolds number, and drag function used with the drag models are as shown in equation (5.1), (5.2), and (5.3). All the calculations are done using SI-units. [28]

$$\mathbf{F}_p = m_p D_f (\mathbf{u}_f - \mathbf{u}_p) \quad (5.1)$$

$\mathbf{F}_p$  is the force acting on a particle,  $m_p$  is the mass of the particles,  $D_f$  is the drag function,  $\mathbf{u}_f$ , and  $\mathbf{u}_p$  is the velocity for the fluid and particle, respectively. [28]

$$Re = \frac{2 \rho_f r_p |\mathbf{u}_f - \mathbf{u}_p|}{\mu_f} \quad (5.2)$$

$\rho_f$  is the fluid density and  $r_p$  is the particle radius. [28]

$$D_f = \frac{3}{8} C_d \frac{\rho_f |\mathbf{u}_f - \mathbf{u}_p|}{\rho_p r_p} \quad (5.3)$$

The  $C_d$  in equation (5.3), is the drag coefficient calculated by the drag models. [28]

Wen-Yu drag model is based on a dependency for fluids volume fraction to account for particle packing and on single-particle drag models. The drag coefficient for Wen-Yu is a function of the Reynolds number with conditions, as shown in equation (5.4). [28]

$$C_d = \begin{cases} \frac{24}{Re} \theta_f^{n_0} & Re < 0.5 \\ \frac{24}{Re} \theta_f^{n_0} (c_0 + c_1 Re^{n_1}) & 0.5 \leq Re \leq 1000 \\ c_2 \theta_f^{n_0} & Re > 1000 \end{cases} \quad (5.4)$$

$c_0$ ,  $c_1$ ,  $c_2$ ,  $n_0$ , and  $n_1$  are the model parameters that can be adjusted. The default values for the model parameters are as shown in Table 5.3.  $\theta_f$  from the equation (5.4) is the fluid volume fraction. [28]



## 5 CPFD Model Development

Table 5.3: Wen-Yu drag model parameters at the default value. [28]

Parameter	Value
$c_0$	1.0
$c_1$	0.15
$c_2$	0.44
$n_0$	-2.65
$n_1$	0.687

The Ergun drag model provided by Barracuda is derived using data from systems with dense beds. Thus simulations with the use of Barracudas parameters are only valid with systems of similar denseness in the bed. [28]

The Ergun drag model calculates the drag function directly and is, as shown in equation (5.5). The calculated drag function is then implemented in equation (5.1). [28]

$$D_f = 0.5 \left( \frac{c_1 \theta_p}{\theta_f Re} + c_0 \right) \frac{\rho_f |\mathbf{u}_f - \mathbf{u}_p|}{\rho_p r_p} \quad (5.5)$$

Barracudas default values for the drag model parameters are as shown in Table 5.4. There are other recommended values for the drag model parameters, and they are 1.75 and 150 for  $c_0$  and  $c_1$  respectively. [30]

Table 5.4: Ergun drag model parameters at the default value. [28]

Parameter	Value
$c_0$	2.0
$c_1$	180

WenYu-Ergun drag coefficient takes the strong points from both the drag models and uses them. Wen-Yu's drag model is for dilute systems, and the Ergun drag model is for systems with dense beds. This blend of drag models is controlled with the conditions set by the particle volume fraction and close pack volume fraction. The equation with the conditions is shown in equation (5.6). [28]

$$D_f = \begin{cases} D_1 & \theta_p < 0.75 \theta_{CP} \\ (D_2 - D_1) \left( \frac{\theta_p - 0.75 \theta_{CP}}{0.85 \theta_{CP} - 0.75 \theta_{CP}} \right) + D_1 & 0.75 \theta_{CP} \geq \theta_p \geq 0.85 \theta_{CP} \\ D_2 & \theta_p > 0.85 \theta_{CP} \end{cases} \quad (5.6)$$

The model parameter explanation can be found in Table 5.5.

## 5 CPFD Model Development

Table 5.5: WenYu-Ergun drag model blend, parameter explanation. [28]

Parameter	Explanation
$\theta_{CP}$	Close Pack Particle Volume Fraction
$D_1$	Drag function (5.3) solved with Wen-Yu drag model (5.4)
$D_2$	Ergun drag function (5.5)

The Turton-Levenspiel model utilizes a single particle drag function with the dependence on the fluid volume fraction. The Turton-Levenspiel drag coefficient can be calculated using equation (5.7), and then the same equations as used for Wen-Yu to find the force acted upon the particles. [28][31]

$$C_d = \frac{24}{Re} (c_0 + c_1 Re^{n_1}) \theta_f + \frac{c_2}{1 + c_3 Re^{n_2}} \theta_f^{n_0} \quad (5.7)$$

The model parameters are shown in Table 5.6.

Table 5.6: Turton-Levenspiel drag model parameters at the default value. [28]

Parameter	Value	Parameter	Value
$c_0$	1.0	$n_0$	-2.65
$c_1$	0.173	$n_1$	0.657
$c_2$	0.413	$n_2$	-1.09
$c_3$	16300		

Non-spherical Haider-Levenspiel is dependent on the fluid volume fraction, and it is derived on the principle of single-particle drag function. The Non-spherical Haider-Levenspiel drag model is including the particle sphericity in the equation. The drag model is shown in equation (5.8). [28][32]

$$C_d = \theta_f^{n_0} \left[ \frac{24}{Re} [1 + c_0 \exp(n_1 \Phi) Re^{(n_2+n_3 \Phi)}] + \frac{24 c_1 \exp(n_4 \Phi) Re}{Re + c_2 \exp(n_5 \Phi)} \right] \quad (5.8)$$

## 5 CPFD Model Development

The drag model parameters are shown in Table 5.7.

Table 5.7: Non-spherical Haider-Levenspiel drag model parameters at the default value. [28]

Parameter	Value	Parameter	Value
$c_0$	8.1716	$n_2$	0.0964
$c_1$	3.0704	$n_3$	0.5565
$c_2$	5.378	$n_4$	-5.0748
$n_0$	-2.65	$n_5$	6.2122
$n_1$	-4.0655		

Figure 5.9 includes all the drag models simulated with their mentioned parameters and conditions. Figure 5.10 shows the drag models compared with the “Experiment Cold-BFB” from Chapter 4.1.3.

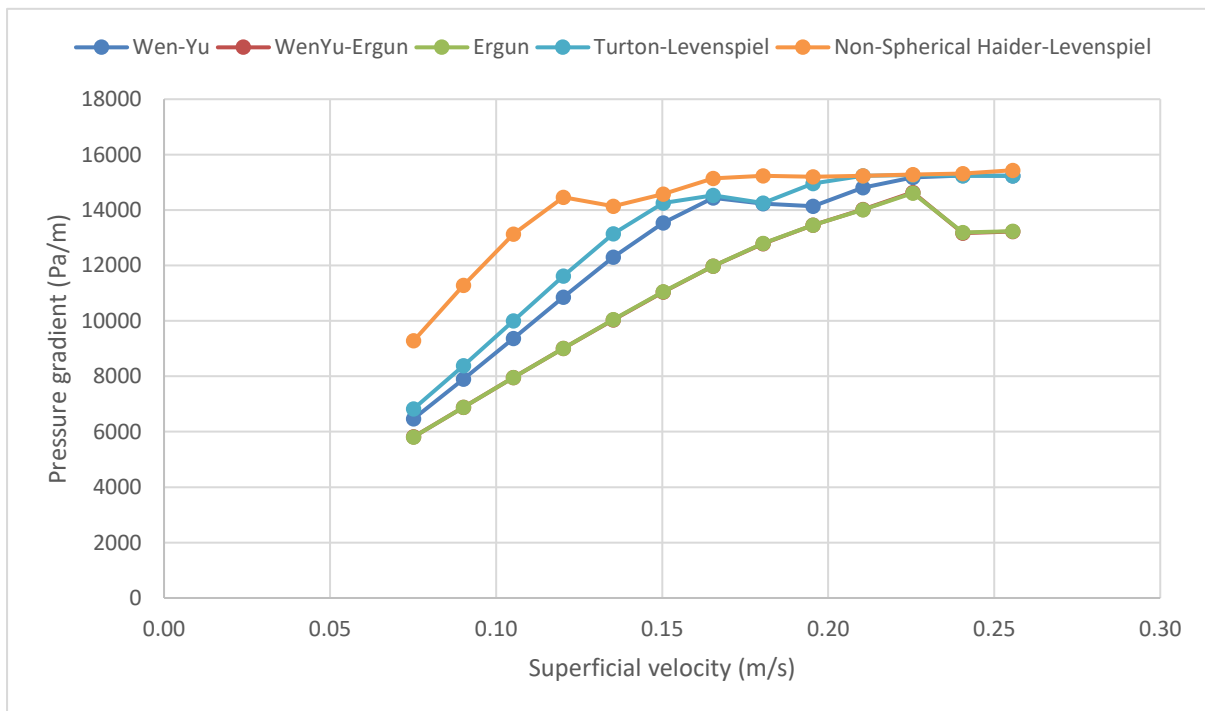


Figure 5.9: Drag model test, Cold-BFB model: drag models compared to each other.

## 5 CPFD Model Development

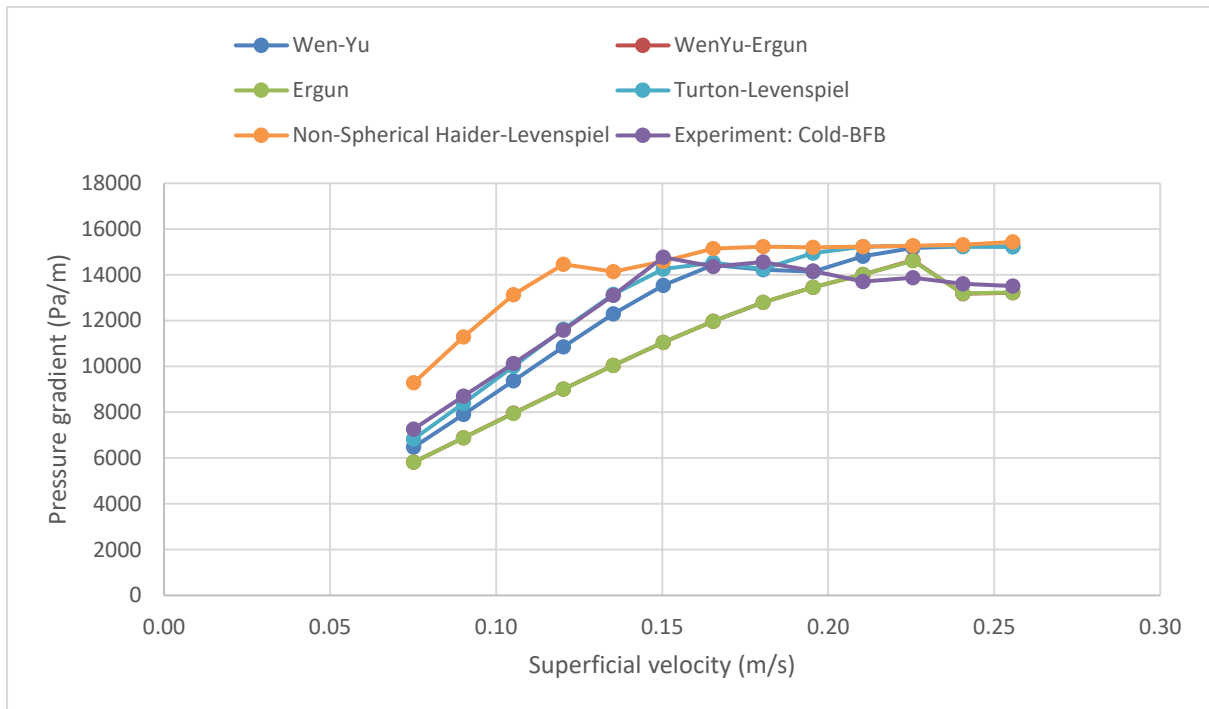


Figure 5.10: Drag model test, Cold-BFB model: drag models compared to each other, including “Experiment Cold-BFB”.

Based on the results from Figure 5.10, the models that adapted the experimental value best were the Wen-Yu drag model and the Turton-Levenspiel drag model. Figure 5.11 shows the two most adapted drag models compared with the “Experiment Cold-BFB”.

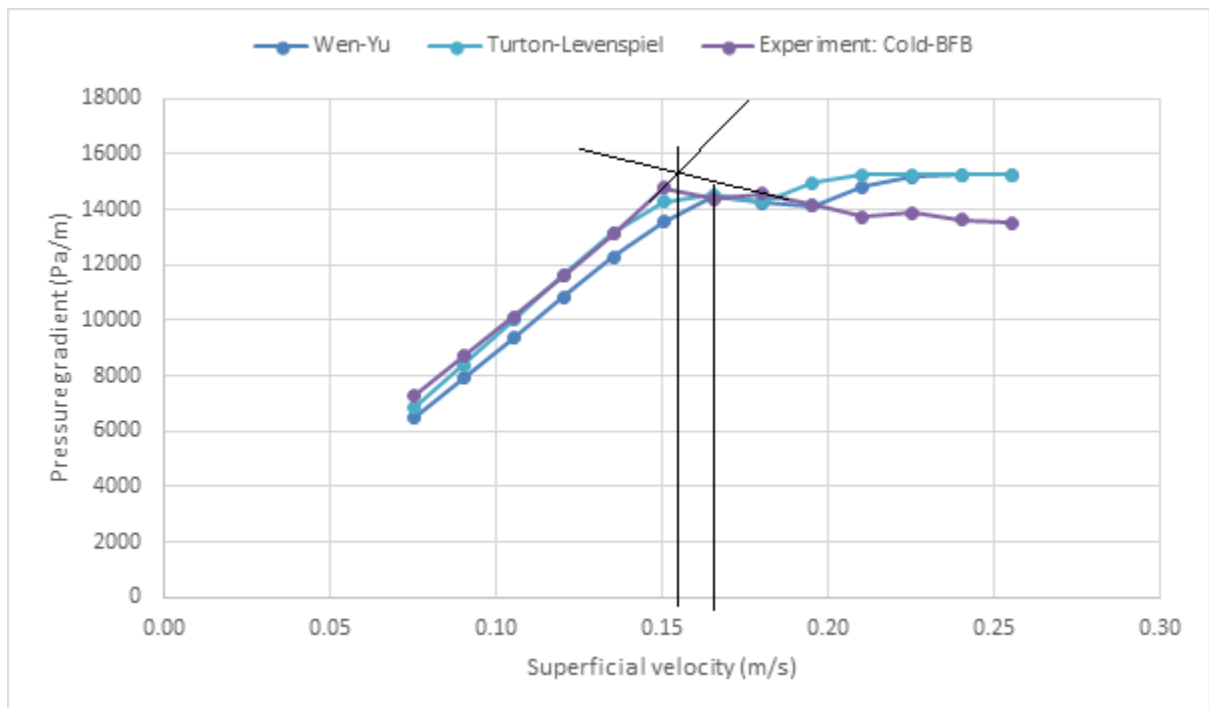


Figure 5.11: Drag model test, Cold-BFB model: selected drag models compare with the experimental results for Cold-BFB, including the locations of minimum fluidization velocities.

Both drag models give a minimum fluidization velocity of roughly 0.17 m/s. The Turton – Levenspiel drag model does match better in the non-fluidized area, but increases in pressure drop after the experiments minimum fluidization velocity. Because of this, Wen-Yu drag model was used in further research.

### 5.3.2 Testing of Various Parameters

Parameter testing was to check how some chosen parameters would affect the model and to make the model more adaptive to the experimental model. The tested parameters were close pack volume fraction, the time duration for each air velocity, normal to wall retention, grid resolution, sensor location, various dispersions of the PSD, and timestep. All results are presented in the form of graphs. The results are also compared with both the Wen-Yu model and the “Experiment: Cold-BFB” curve. The Wen-Yu from Figure 5.11 is referred to as “Base Case” in these graphs.

The CPVF was tested on how much it is affecting the model. Figure 5.12 shows the simulated results where the volume fraction was changed from 0.6 to 0.63.

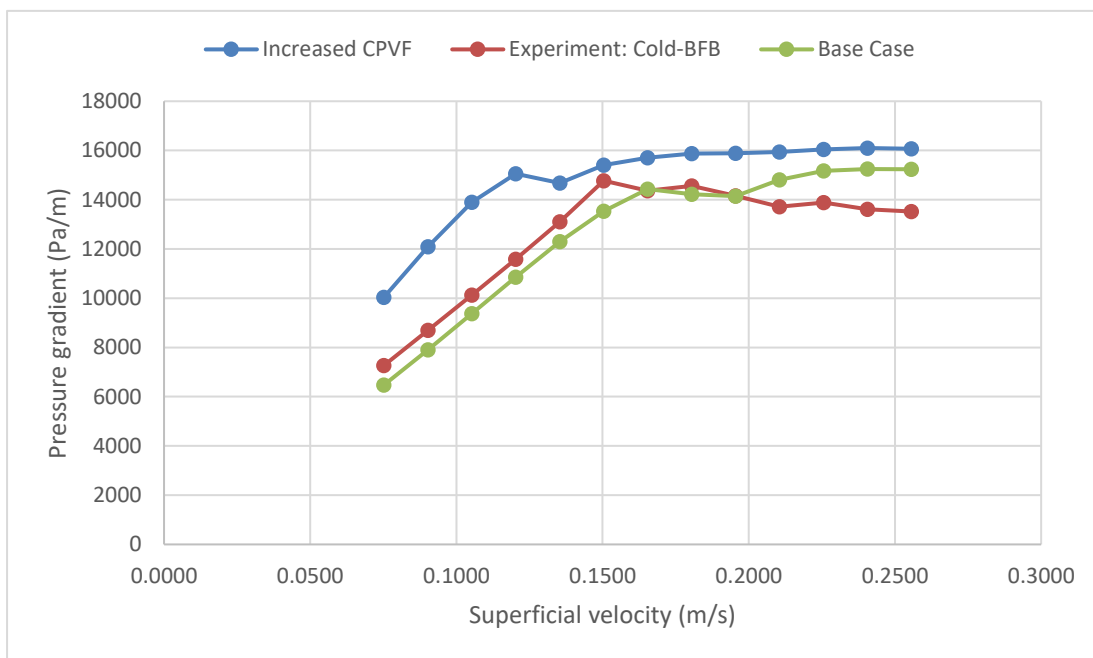


Figure 5.12: Parameter test, Cold-BFB model: increased close pack volume fraction compared with Base Case and experimental data.

The model is hypersensitive to changes in the CPVF; a change of 0.03 had a dramatic impact. This sensitivity was anticipated as the Wen-Yu equation (5.4) is shown to be dependent on the fluid volume fraction.

The velocity duration was adjusted in the flow BC Table 5.1. Instead of a 5-second incrementation, it was changed to 10-second incrementation. The adjusted incrementation makes so the velocity stays active for a more extended period before changing. The simulation result is shown in Figure 5.13.

## 5 CPFD Model Development

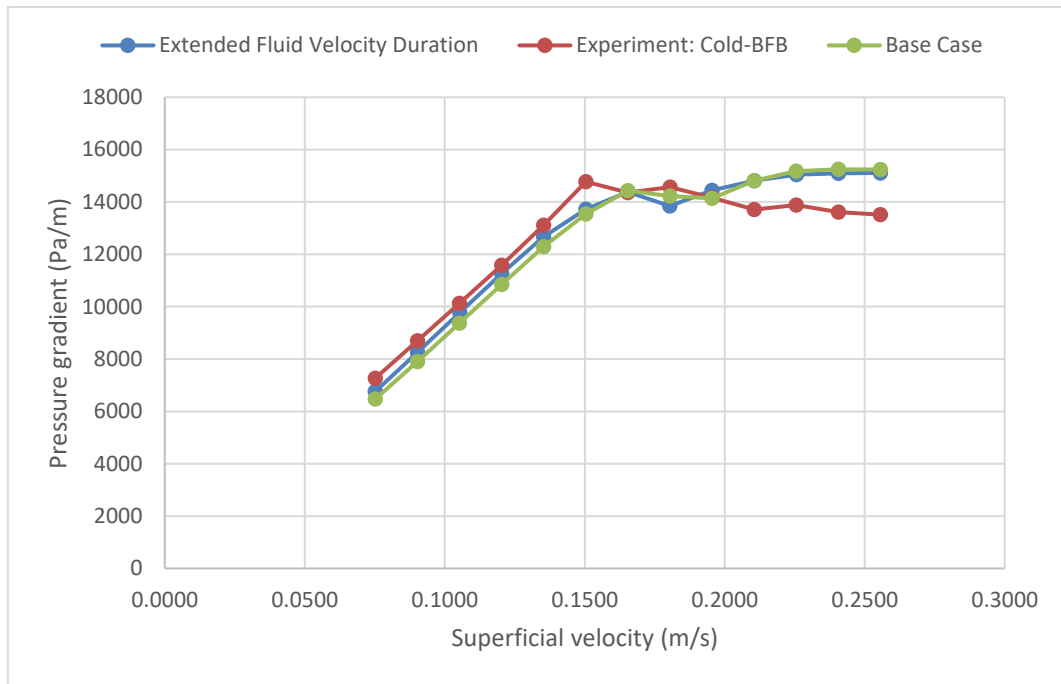


Figure 5.13: Parameter test, Cold-BFB model: extended fluid velocity duration compared with Base Case and experimental data.

The extended fluid velocity duration made some improvements in adaptation. The computational time increased significantly.

The normal to wall retention was changed from 0.85 to 0.4. The simulated result can be seen in Figure 5.14.

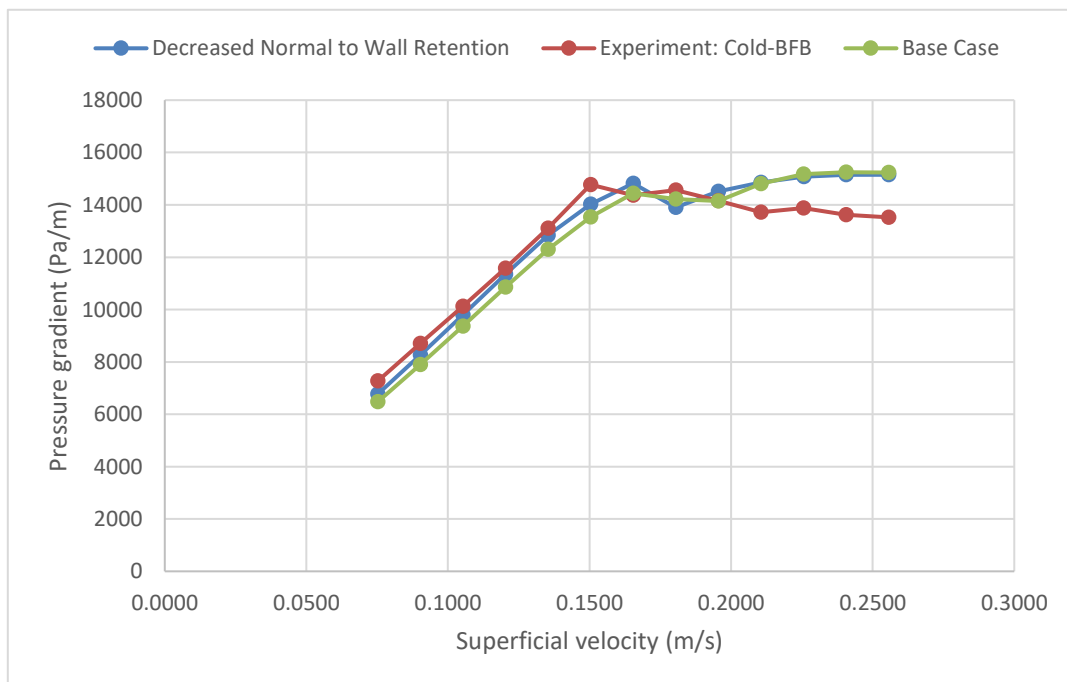


Figure 5.14: Parameter test, Cold-BFB model: decrease normal to wall retention compared with Base Case and experimental data.

## 5 CFPD Model Development

The normal to wall retention did make the model adapt more evenly, especially at the part before velocity 0.15 m/s.

Lower grid resolution results in less computational cells and less accuracy. Figure 5.15 shows the simulated results when a grid resolution of 4000 total cells, which is adjusted to 3708 uniformly distributed cells.

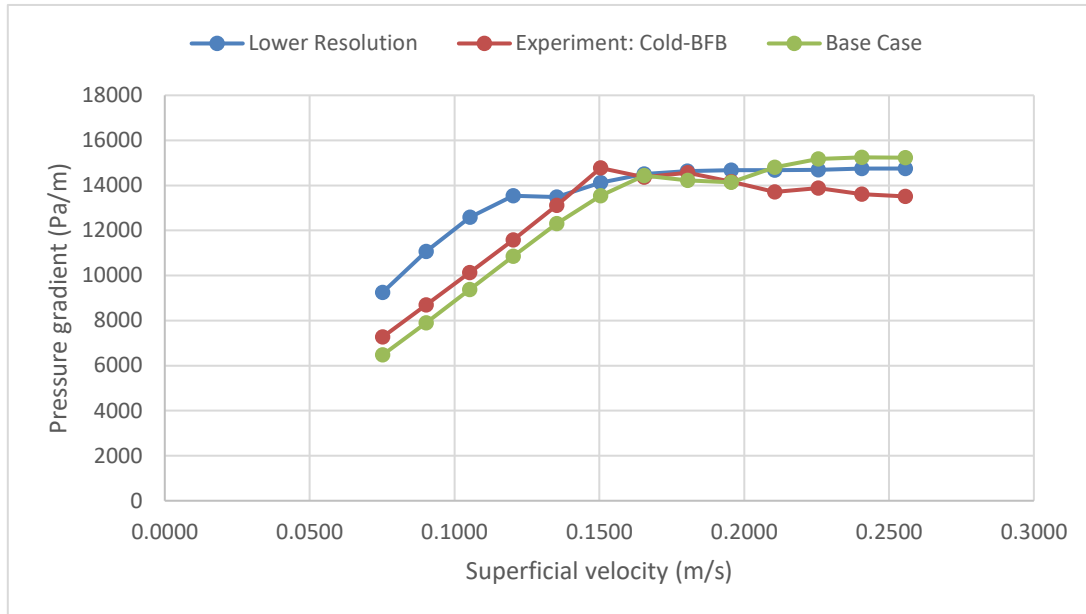


Figure 5.15: Parameter test, Cold-BFB model: lower grid resolution compared with Base Case and experimental data.

As expected, the lower resolution did make the model less accurate. The number of data processing cells is not sufficient as it is not adapting to the experimental data. The lower grid resolution was only tested to see the magnitude of the impact on the model.

The location for the pressure sensors was tested. The goal was to imitate and compare with the physical sensor locations in the Cold-BFB. Usually, the pressure sensors are placed in the center of the column when simulating as to give the overall average pressure data. The new sensor x- and y- coordinates can be found in Table 5.8. The z coordinates for the sensors remain the same as used in Table 5.2. The simulated results are shown in Figure 5.16.

Table 5.8: Parameter test, Cold-BFB model: new coordinates for pressure sensors.

Sensor number	Coordinates [x,y,z]
Pressure Sensor 1	[0.01, 0.0423, 0.035]
Pressure Sensor 2	[0.01, 0.0423, 0.135]

## 5 CPFD Model Development

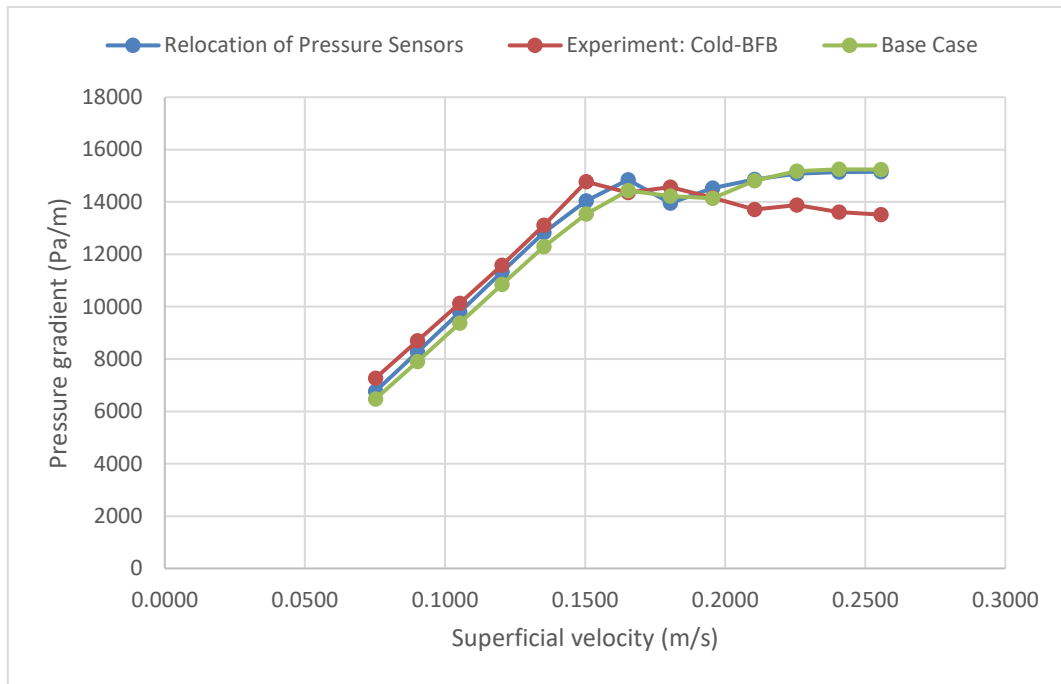


Figure 5.16: Parameter test, Cold-BFB model: Relocation of pressure sensors compared with Base Case and experimental data.

The relocation of the sensors did provide an improvement in the model adaptation.

The timestep was changed from 0.001 s to 0.0001 s. Decreasing the timestep increases the calculation per incrementing change in time. It also increases the possibility of capturing more fluctuations and making the model more adaptive. A smaller timestep increases the computational time. Figure 5.17 shows the simulated results.

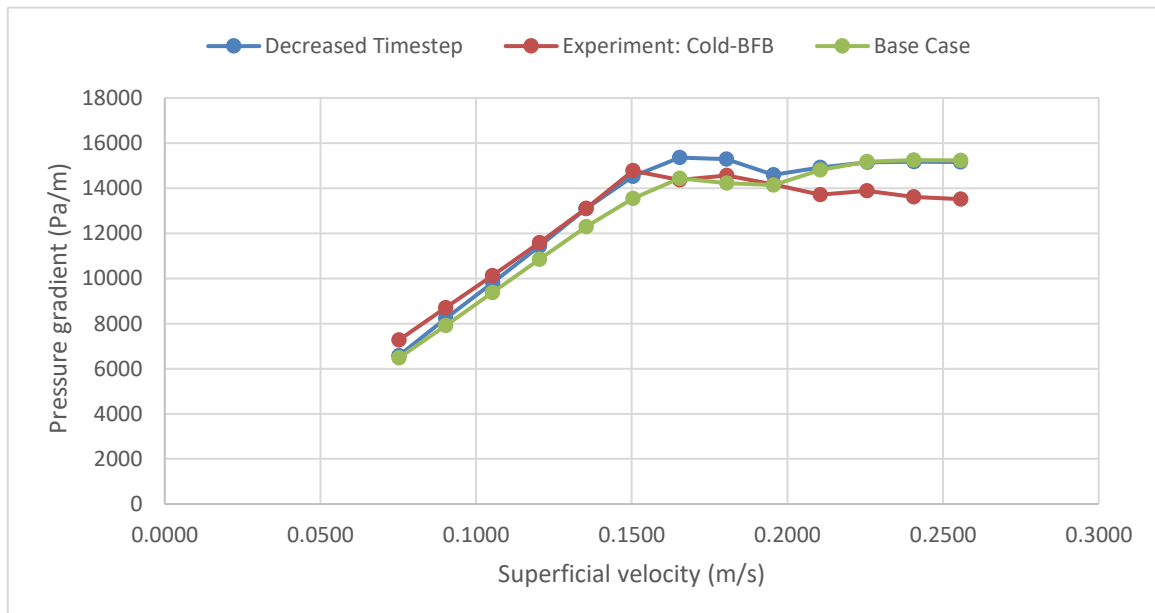


Figure 5.17: Parameter test, Cold-BFB model: decreased timestep compared with Base Case and experimental data.



## 5 CFPD Model Development

Lower timestep gave the model almost no deviation in the non-fluidized part and an overall increase in pressure gradient. The model does overshoot after the experiments minimum fluidization velocity.

A finer resolution with a lower timestep was simulated to see if there would be any notable changes in the model. The resolution used is 20000 total cells, which converts to 17700 uniformly distributed cells, and a timestep of 0.0001 s. The results are shown in Figure 5.18.

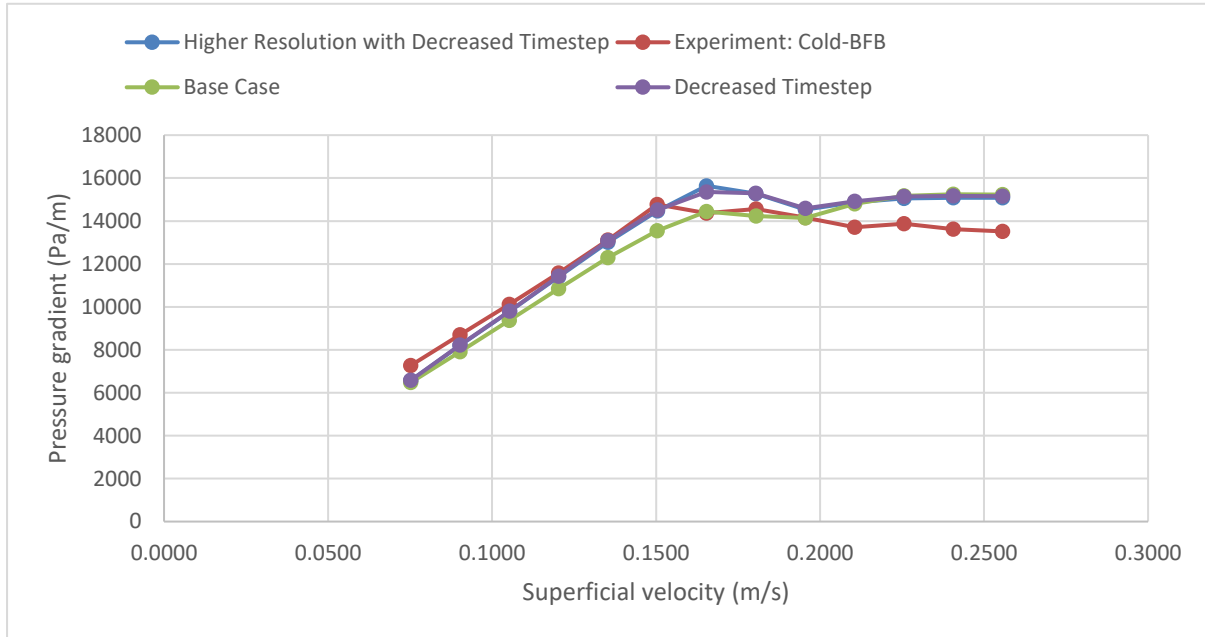


Figure 5.18: Parameter test, Cold-BFB model: finder grid resolution with decreased timestep compared with Base Case and experimental data.

The changes are minimal compared with the results where only the timestep was changed. This small change is not worth it in regards to the increased computational time.

A variety of PSD was simulated to see how the model would act with different dispersions in size distributions. It was tested with a cumulative percentage favoring the upper and lower PSD with the mean particle size from Chapter 4.1 as a referencing point. The model was also simulated with only the mean particle size. The distribution sheets used can be found in Appendix C. The timestep is 0.0001 s, but the grid resolution is changed back to the initial value from Chapter 5.2.3. The PSD test is shown in Figure 5.19.

## 5 CFPD Model Development

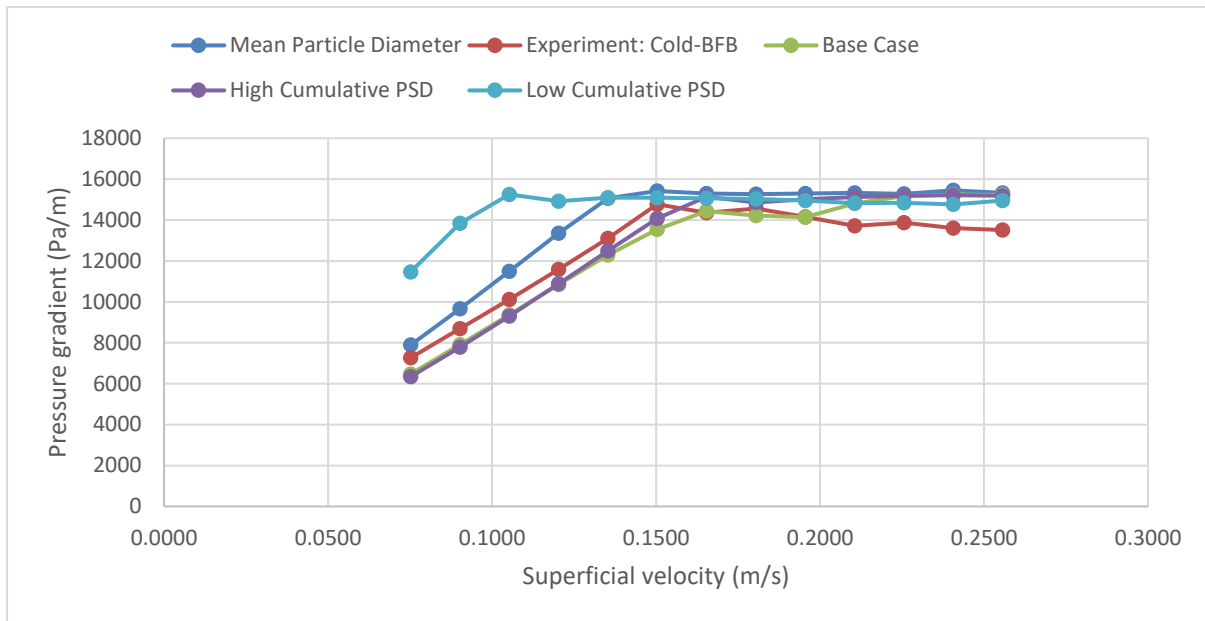


Figure 5.19: Parameter test, Cold-BFB model: PSD test, which includes a more narrowed size distribution and a mean particle size compared with Base Case and experimental data.

The PSD test shows that the significant deviation occurring after 0.2 m/s in the previous simulations may be because of a wide PSD dispersion.

Out of the drag model tests and parameter tests, the timestep of 0.0001 s and the Wen-Yu drag model is chosen to be used for further testing in BFB-gasifier. The rest of the parameters remains, as initially mentioned in Chapter 5.2.

### 5.4 BFB-Gasifier Model

The model developed for Cold-BFB is used to simulate the BFB-gasifier with the experimental parameters and results from Chapter 4.2.

The geometry for the reactor is 0.1 m in diameter and 1 m in height. The grid has 12000 in total cells and 10600 in uniformly distributed cells. The cell layout is, as shown in Figure 5.20.

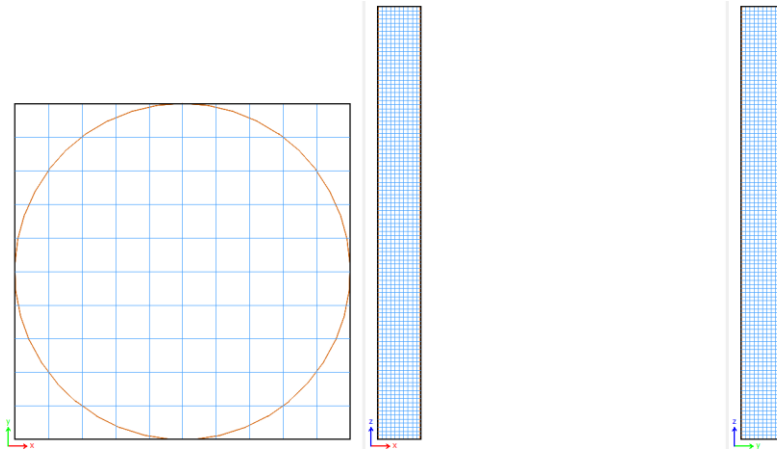


Figure 5.20: BFB-gasifier: grid layout presented in 2-D.

The pressure sensors are located in the center of the geometry with the same z-coordinates used in both experiments. Table 5.9 shows the coordinates, and Figure 5.21 shows the locations in the geometry.

Table 5.9: Parameter, BFB-gasifier: pressure sensor coordinates.

Sensor number	Coordinates [x,y,z]
Pressure Sensor 1	[0.05, 0.05, 0.035]
Pressure Sensor 2	[0.05, 0.05, 0.135]
Pressure Sensor 3	[0.05, 0.05, 0.143]
Pressure Sensor 4	[0.05, 0.05, 0.238]

The pressure sensors are paired up when simulating, and the pairs are  $P_1$  and  $P_2$  ( $P_3$  and  $P_4$ ) for simulation case 1 (simulation case 2).

## 5 CPFD Model Development



Figure 5.21: BFB-gasifier: pressure sensor locations in the geometry.

The sand size distribution is shown in Figure 5.22, the temperature is 1008 kelvin, and the particle volume fraction is 0.5497. The simulated BFB-gasifier data are shown in Figure 5.23.

Particle Size Distributions Editor

	Cumulative (%)	Radius (m)
1	0	0.0001
2	28.64	0.00015
3	56.00	0.000213
4	66.11	0.00025
5	95.24	0.0003
6	100	0.00035

Figure 5.22: Parameter, BFB-gasifier: PSD sheet.

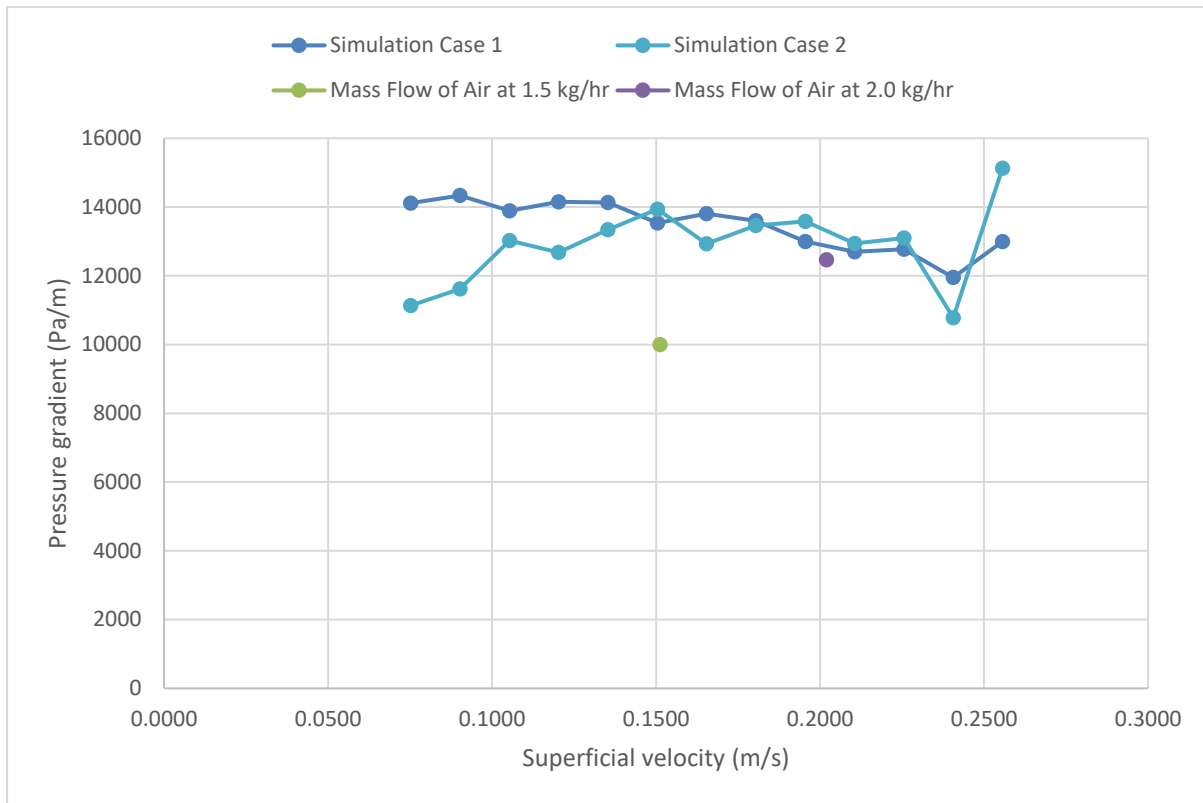


Figure 5.23: Simulation, BFB-gasifier: simulated data compared with the experimental data from the BFB-gasifier.

The experimental data point for the mass flow of air at 1.5 kg/hr is deviating from the model. The deviation is thought to be because of the location of sensor  $P_4$ . The  $P_4$  sensor is located at a height of 0.238 m, while the fixed bed has a height of 0.2 m. The height difference between  $P_4$  and the fixed bed could lead to pressure readings when there is no bed material between the sensors in simulation case 2. The mass flow of air at 2.0 kg/hr and simulation case 1 reasonably close, thus making the model used in further research with agglomerates.

## 5.5 Set-Up For Insertion of Agglomerates

Agglomerates are considerably larger than the bed particles. Thus a bigger geometry is needed to simulate an agglomerated bed. The BFB-gasifier is scaled to a pilot-sized gasifier with the use of Glicksman's scaling rules.

### 5.5.1 Bed Parameters and CFPD Parameters for the Pilot-Scale

As a start for the up-scaling, the diameter of the pilot-scaled reactor was chosen to be 0.5 m. The condition for the viscous limit in Glicksman's scaling rules is satisfied as the Reynolds number equals to 0.79. The density and the viscosity in the Re equation were at 735 °C for air. The velocity was chosen to be 0.26 m/s, as it is the highest superficial velocity used in simulations and experiments.

The length dimension ratio  $L_1/L_2$  from equation (3.3) gives the scaling factor 5. With this scaling factor, the rest of the Glicksman's ratios from equation (3.3) is calculated and gives the

## 5 CPFD Model Development

results, as shown in Table 5.10. Glicksman's dimensionless parameter  $L/d_p$  was neglected in this study.

Table 5.10: Glicksman's scaling parameters: BFB-gasifier to Pilot-Size dimensions.

Parameters	Lab-Scale (2)	Pilot-Scale (1)	Unit
$D$	0.1	0.5	$m$
$H$	1	5	$m$
$h$	0.2	1	$m$
$T$	735	735	$^{\circ}C$
$\rho_p$	2650	2650	$\frac{kg}{m^3}$
$\rho_g$	0.35	0.35	$\frac{kg}{m^3}$
$\mu_g$	4.2e-5	4.2e-5	$\frac{kg}{m\ s}$
$u_{mf}$	0.051	0.114	$\frac{m}{s}$
$u_0$	0.153	0.342	$\frac{m}{s}$
$L$	0.1	0.5	$m$
$Froude$	0.024	0.024	—
$\bar{d}_p$	367	549	$\mu m$

The  $u_0$  from Table 5.10 is three times the minimum fluidization velocity. The bed volume for the pilot-scale equals to  $0.2\ m^3$ .

The CAD geometry has the dimensions 0.5 m in diameter and 5 m in height. Grid resolution with a similar uniformly distributed cell count as the BFB-gasifier grid was used for the pilot-scale. The grid resolution is 10200 total cells and 10000 uniformly distributed cells. The cell layout is shown in Figure 5.24.

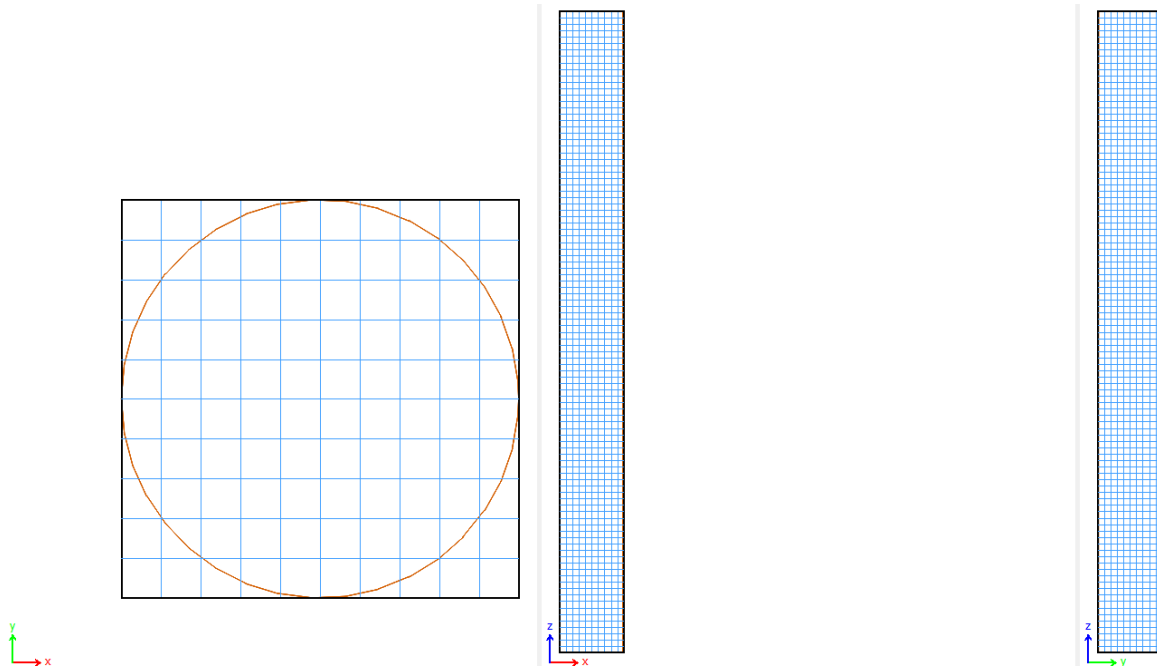


Figure 5.24: Pilot-Scaled Gasifier: grid layout presented in 2-D.

This grid resolution provides cells with a physical size of 5 cm. The pressure sensor locations are at the same x- and y-direction as the  $P_1$  and  $P_2$  used in Table 5.2, but the z-direction is scaled up using scaling factor 5. The coordinates are as shown in Table 5.11.

Table 5.11: Parameter, Pilot-Scaled Gasifier: pressure sensor coordinates.

Sensor number	Coordinates [x,y,z]
Pressure Sensor 1	[0.25, 0.25, 0.175]
Pressure Sensor 2	[0.25, 0.25, 0.675]

### 5.5.2 Confirming the Pilot-Scaled Gasifier

The first simulation was performed to see if the scaling was done correctly. The simulated velocities were scaled up from Table 5.1 with the use of the Froude number for each velocity. The minimum fluidized velocity was found by adding extra increments in the flow BC. The added velocities are from 0.015 m/s to 0.101 m/s with a increase of 0.005 m/s. The simulation is shown in Figure 5.25. The velocities used in flow BC is shown in Appendix D.

## 5 CPFD Model Development

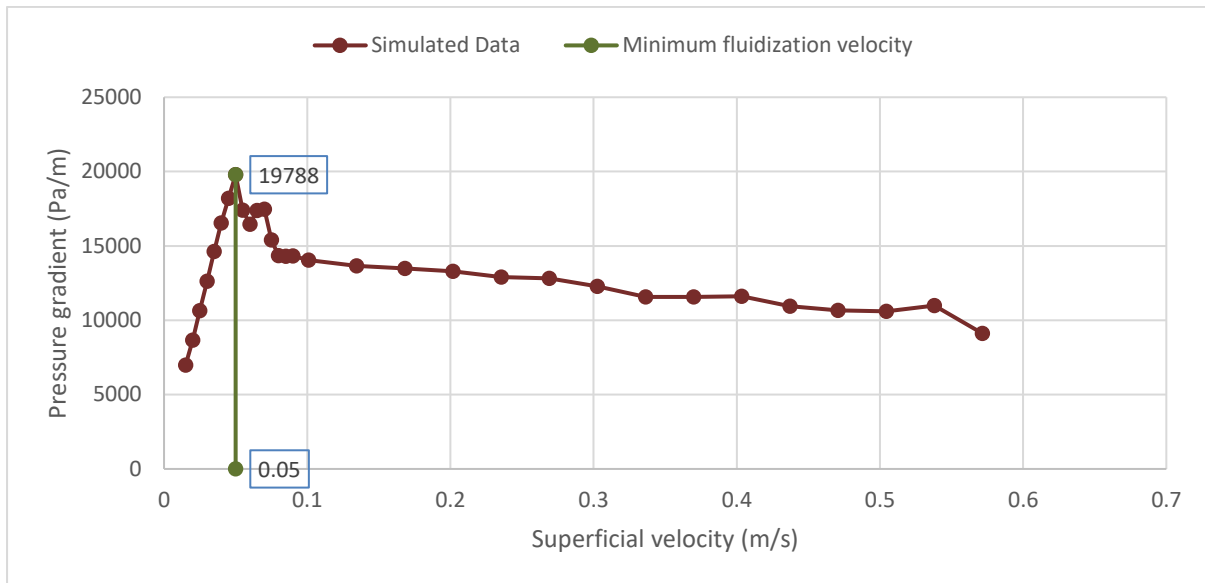


Figure 5.25: Simulation, Pilot-Scaled Gasifier: simulated data with the localization of the minimum fluidized velocity.

The minimum fluidization velocity was found to be at 0.05 m/s, and account for a deviation of 56% when compared with the scaled value of 0.114 m/s. The deviation may be caused by the neglect of the dimensionless parameter  $L/d_p$ . For simplicity, the scaling was accepted and used for further simulations.

### 5.5.3 Injection Set-Up

Injection of agglomerates is used to find out how much agglomerates are needed in the bed to make a difference in the pressure gradient. Figure 5.26 shows how Injection BC is configured. The flow BC in the model were changed to run at a single velocity of 0.15 m/s.

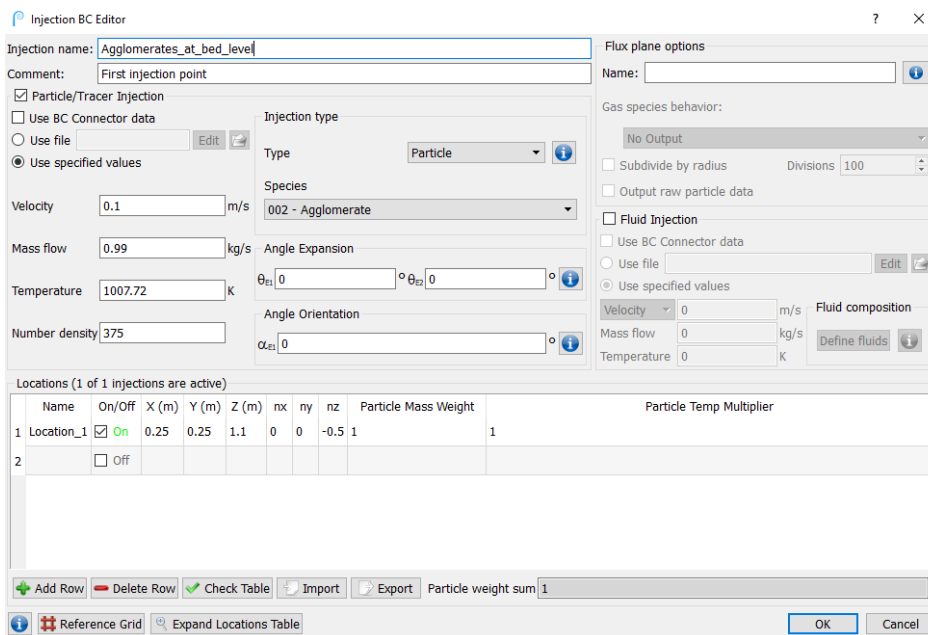


Figure 5.26: Parameter, Pilot-Scaled Gasifier: used injection settings in Barracuda



## 5 CFPD Model Development

The injection velocity is 0.1 m/s to minimize the influence of the agglomerates when entering the bed. The temperature is the same as the operating temperature inside the scaled-reactor. The agglomerates are created as a new species. They are specified as a specie with a density of  $1506 \text{ kg/m}^3$ , size between 3-4 cm in diameter, and asphericity of 0.4. The agglomerates particle sphericity of 0.4 was based on visual and tactile data. The mass flow was calculated by assuming that the flow behavior in the bed would be affected when a volume of agglomerates corresponding to 10% of the bed is present. 10% of the bed volume equals 29.6 kg of agglomerates. The weight is calculated by using the density of  $1506 \text{ kg/m}^3$  for agglomerates. It was decided to reach 29.6 kg after 30 seconds of simulation time, and the total simulation time would go to 90 seconds. At the end of the simulation, roughly 90 kg of agglomerates would be in the reactor, making it overshoots in case 29.6 kg was not enough to affect the flow behavior.

The location of the injection point is adjusted by X(m), Y(m), and Z(m), while  $n_x$ ,  $n_y$ , and  $n_z$  is the injections nozzle direction. The agglomerates are programmed to be injected downwards, and 10 cm over the center-top of the bed. The number density was tested to see how it would affect the injection simulation, the test between the default value of 125 and 375 can be found in Appendix E. Number density 375 was used at the final simulation. The rest of the parameters are at default values. The injection nozzle can be seen in Figure 5.27.

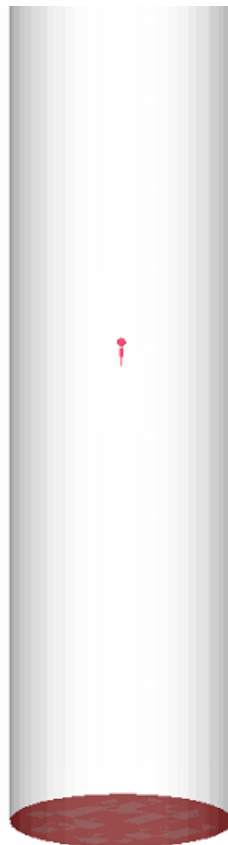


Figure 5.27: Pilot-Scale Gasifier: injection location in the geometry with nozzle direction.

## 6 Results and Discussion

This chapter covers the results, analysis, and validation of the CPFD model. The chapter also includes simulations with agglomerates and discussions alongside the presented data.

### 6.1 Comparison Between Experimental and Simulated Results

The drag models and the parameters tested in Chapter 5.3, were evaluated with model adaptation and computational time as a deciding factor. The parameters: extended fluid velocity duration, decreased timestep, normal to wall retention, and the pressure sensor location gave improved adaptation for the CPFD model. The normal to wall retention and the pressure sensor location showed that they do have an impact on the model and is thus important to take into account when developing a CPFD model for a bubbling fluidized bed. Because of insufficient time, there was chosen only to use one of the parameters when simulating. For the simulation model, it was decided to use the decreased timestep of 0.0001 s and the Wen-Yu drag model with the initial parameters presented in Chapter 5.2. The model is shown as “Simulated Model: Cold-BFB” in Figure 6.1, where it is compared with the results from the Cold-BFB experiment.

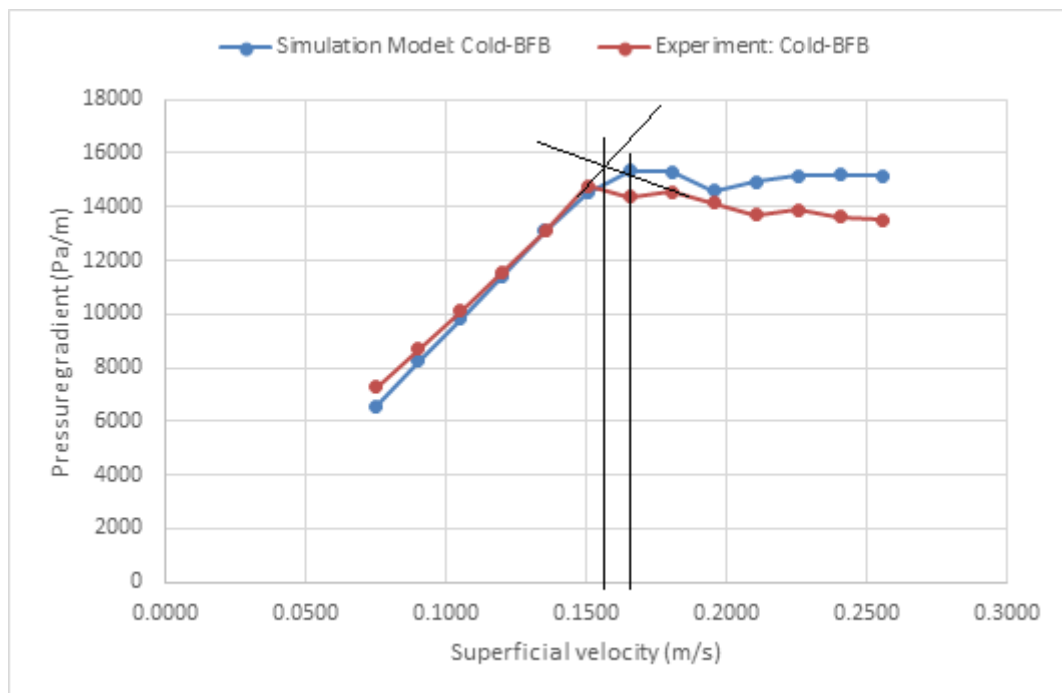


Figure 6.1: Result, Cold-BFB model: model validation with the locations of minimum fluidization velocities.

The highest deviation in the pressure gradient between the simulated data and the experimental data is 12 %, and it is after the superficial velocity of 0.195 m/s. The average deviation in the model is 6 %. The minimum fluidization velocity is 0.16 m/s and 0.17 m/s for the experiment and the simulation, respectively. The deviation in the minimum fluidization velocity equals to roughly 6 %. The overall deviation can be related to the numerical method MP-PIC and the drag model parameters. MP-PIC does not track and solve for each particle. The numerical method uses an approach where the particles with equal properties are grouped and represented as one computational particle. The other possible reason for the overall deviation is the flawed

## 6 Results and Discussion

assumption that the drag model parameters are sufficient at the default values. Due to insufficient time, the parameters for each model were left at default values. The parameters for each drag model have the potential to be adjusted and compared for better model adaptation. The Ergun drag model is often recommended to use other parameters, as mentioned in Chapter 5.3.1. These parameters were not tested, as explained earlier.

The 12 % deviation after the superficial velocity of 0.195 m/s could be because of a wide PSD. The PSD testing presented in Figure 5.19 provided some argument for the significant deviance in pressure gradient after the minimum fluidization velocity could be due to a wide PSD. There was tested a narrower PSD in both higher and lower PSD range with the mean particle size as a referencing point. The PSD test sheets can be found in Appendix C. This showed that when the PSD was more narrowed, the deviance would not be so significant in the fluidized region, as shown in Figure 6.1.

The model was then tested with the BFB-gasifier's geometry, particle properties, IC, and BC. There is only used one experimental velocity point to compare and validate the CPF model, as shown in Figure 6.2. The flow BC chart can be found in Appendix D

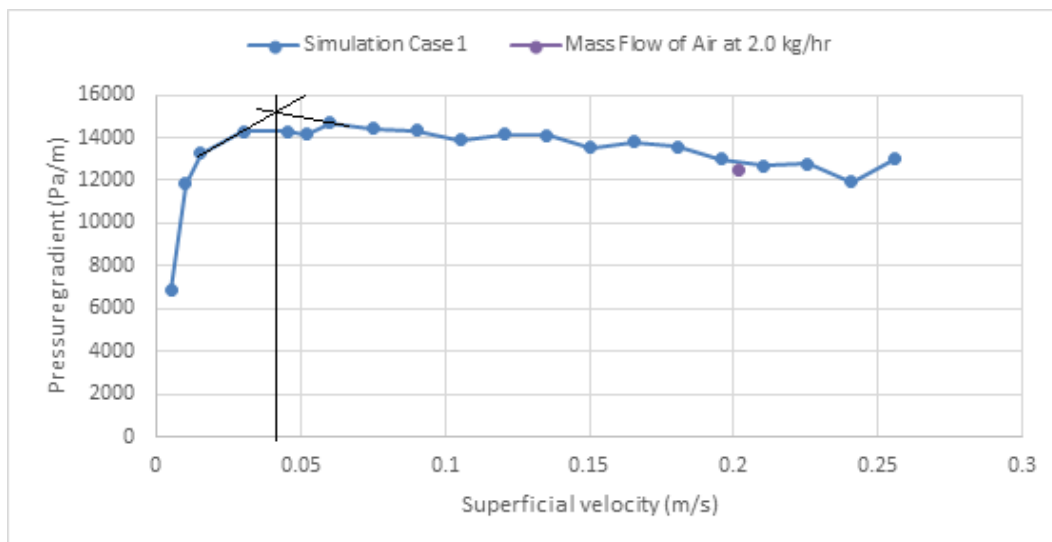


Figure 6.2: Result, BFB-gasifier: model validation with the location of minimum fluidization velocity.

The deviation in the pressure gradient between the model and the experiment at a superficial velocity of 0.2 m/s is 3 %. The deviation was found by interpolation between the points (0.195, 12993) and (0.210, 12701) with the experimental point (0.2, 12469). According to equation (2.4), the minimum fluidization velocity is 0.051 m/s, while the simulation show 0.045 m/s, accounting for a 12 % deviation. With the use of a similar air velocity profile, as used in the Cold-BFB experiment, a more detailed comparison between the experimental and simulated data could have been conducted.

The CPF model has shown good results when compared with the experimental data from both the Cold-BFB and BFB-gasifier if an average deviation of 6 % in the pressure gradient, and a maximum deviation of 12 % in the minimum fluidization velocity is acceptable.

## 6.2 Results From Agglomerated Bed

The BFB-gasifier was up-scaled using Glicksman's set of dimensionless parameters at the viscous limit. Glicksman's rules are used to maintain the fluid dynamic similarities between the two scales. However, as mentioned in Chapter 5.5.2, the dimensionless parameter  $L/d_p$  is neglected, and the deviation between the simulations and the Glicksman's  $u_{mf}$  parameter is 55 %. Thus it could be an argument against if the scales have maintained fluid dynamic similarities or not. For simplicity, the scaled version of the BFB-gasifier is accepted. The reason the geometry was scaled was to be able to simulate bigger particles with the same grid resolution throughout the geometries, and the  $L/d_p$  parameter was chosen to be neglected as the bed particle size would have been significantly larger.

Figure 6.3 includes a simulation comparison between a reactor with and without injection of agglomerates. Both the simulations have the same constant flow velocity of 0.15 m/s. In the simulation with agglomerates, the agglomerates are fed to the scaled-reactor at a mass rate of 1 kg/s.

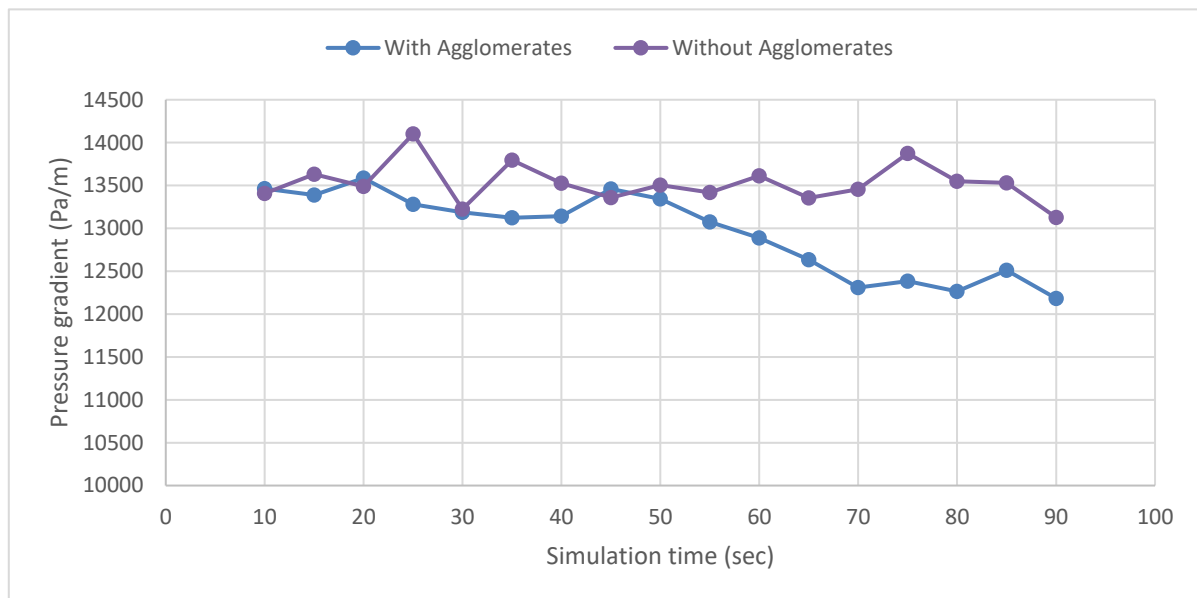


Figure 6.3: Result, Pilot-Scale Gasifier: comparison between simulation with and without agglomerates at a constant velocity.

It can be seen that the decrease in pressure gradient from time 50 to 70 is caused by the agglomerates. 50 to 70 seconds corresponds to roughly 50-70 kg of agglomerates, and 17- 24 % of the bed volume. Figure 6.4 to Figure 6.8 shows how the agglomerates behave as they are injected into the bed, the blue particles are sand, and red is the agglomerates. Figure 6.5, Figure 6.6, and Figure 6.7 show the column with 8 kg, 52 kg, and 60 kg of agglomerates, respectively. Figure 6.7 displays agglomerates making their way towards the bottom of the column; this is a sign of segregation. Figure 6.9 to Figure 6.12 shows the particle volume fraction throughout the bed. From Figure 6.9 to Figure 6.11, it can be seen that after 52 seconds, 52 kg of agglomerates, the particle volume fraction is starting to increase at the bottom of the column.

The increase of both the concentration of agglomerates and the increase of particle volume fraction at the bottom of the reactor could be the reason that the pressure gradient in Figure 6.3 drops at time 50 s. At simulation time 90 seconds, the agglomeration is occupying most of the

## 6 Results and Discussion

column, as seen in Figure 6.8. Figure 6.9 to Figure 6.12, further illustrates the point that the agglomerates are occupying most of the column as the particle volume fraction is very high throughout the column. Figure 6.12 shows restriction for the voids and possible fluid channelings.



Figure 6.4: Result, Pilot-Scale Gasifier: injection at time 0 s.



Figure 6.5: Result, Pilot-Scale Gasifier: injection at time 8 s.

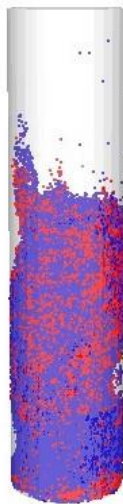


Figure 6.6: Result, Pilot-Scale Gasifier: injection at time 52 s.



Figure 6.7: Result, Pilot-Scale Gasifier: injection at time 60 s.

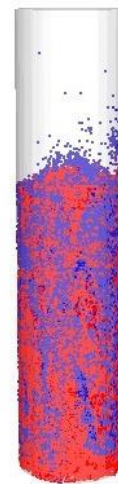


Figure 6.8: Result, Pilot-Scale Gasifier: injection at time 90 s.

## 6 Results and Discussion

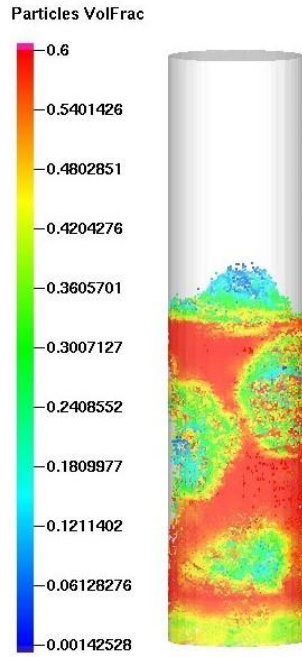


Figure 6.9: Result, Pilot-Scale Gasifier: particle volume fraction at injection time 14 s.

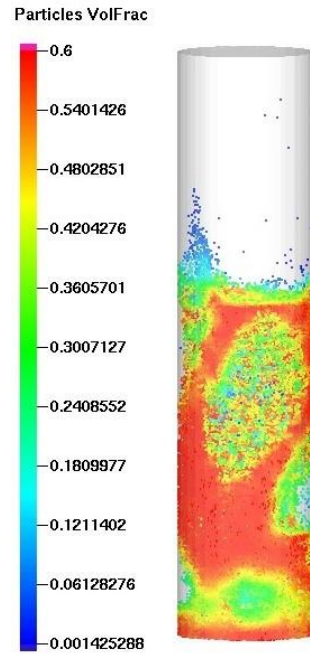


Figure 6.10: Result, Pilot-Scale Gasifier: particle volume fraction at injection time 52 s.

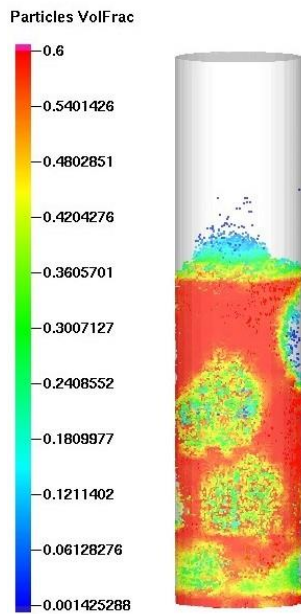


Figure 6.11: Result, Pilot-Scale Gasifier: particle volume fraction at injection time 60 s.

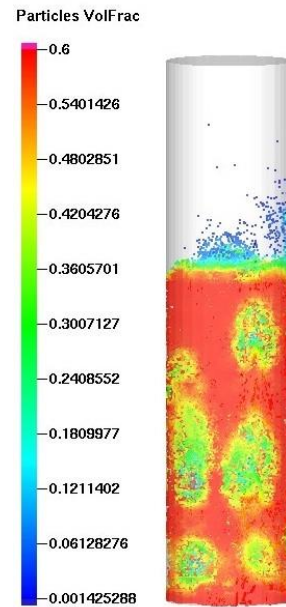


Figure 6.12: Result, Pilot-Scale Gasifier: particle volume fraction at injection time 90 s.

## 6 Results and Discussion

When simulating the agglomerated bed behavior, 60 kg of agglomerates were used. 60 kg was used to be sure that there would be some effect in the flow behavior when simulating. 60 kg of additional agglomerates in the bed makes a total of 345.5 kg. 60 kg of agglomerates is 20% of the initial scaled bed volume and equals  $0.04 \text{ m}^3$ . The volume of the agglomerates makes a height of 0.2 m, and 0.36 m when including the particle volume fraction from Table 4.5. The total height of the bed is then 1.36 m, where 0.36 m is agglomerates. The agglomerates then account for 26 % of the scaled bed volume.

The initial conditions for the agglomerated bed are calculated with the same model parameters as the model from Figure 6.3 at 60 seconds. These are model parameters such as total weight, volume, and particle volume fraction. The model parameters were calculated with respect to the IC of constant particle volume fraction throughout the bed, and that 26 % of the bed volume should be additional agglomerates. The particle volume fraction for agglomerate is 0.14 and 0.41 for sand; this gives a total weight of 345 kg in the bed.

The simulation with an agglomerated bed is shown in Figure 6.13. The agglomerated bed is compared with the pilot-scale simulation without agglomeration from Figure 5.25. The flow BC chart used in this case can be found in Appendix D, and a prolonged version of Figure 6.13 can be found in Appendix E.

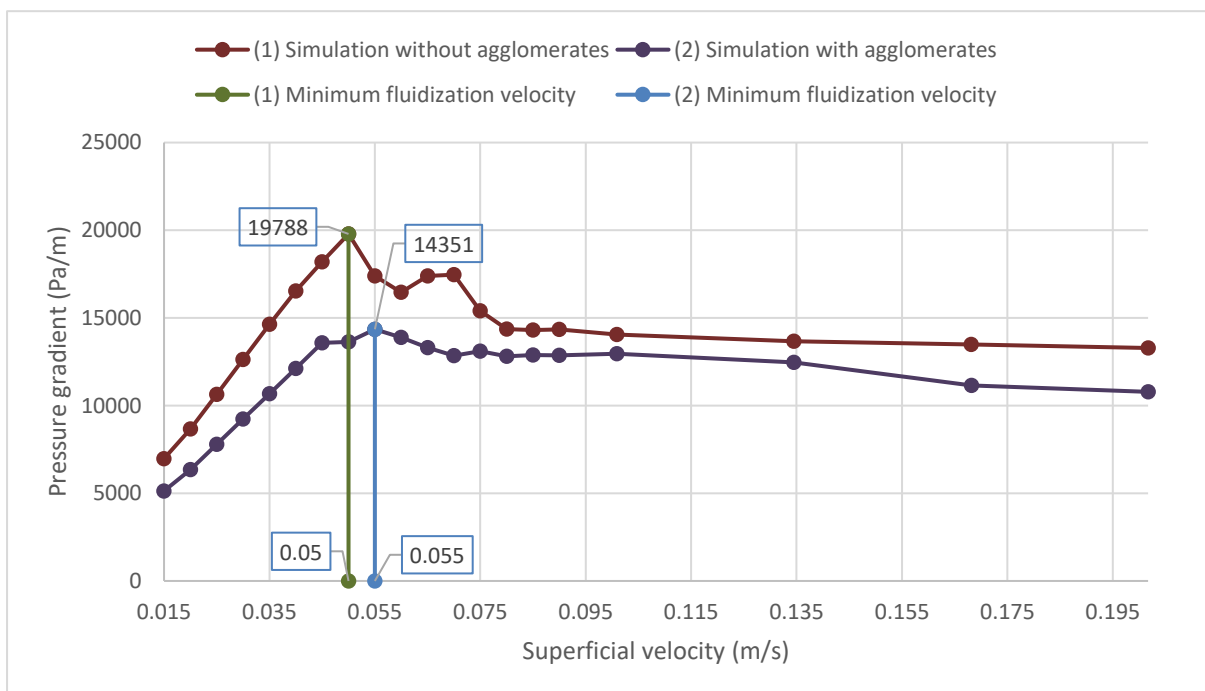


Figure 6.13: Result, Pilot-Scale Gasifier: comparison between the agglomerated bed and the normal bed. Points of minimum fluidization velocities are included.

The bubbling fluidized bed parameters were affected by the agglomerates. The overall pressure gradient over the bed decreased when agglomerates were added to the bed. The minimum fluidization velocity increased when agglomerates were added. The decrease in pressure

## 6 Results and Discussion

gradient illustrates that there is more fluid traveling through the bed; this could be because of the low density that agglomerates have. The simulated data needs to be experimentally validated to become completely trustworthy.

Figure 6.14 and Figure 6.15 shows the position and particle volume fraction for agglomerates at minimum fluidization velocity. Figure 6.14 shows that the agglomerates are traveling downwards when the bed becomes fluidized.

Figure 6.13 and Figure 2.8 display similarity in how an agglomerated bed compares to a regular bed. The similarity regards the pressure gradient and minimum fluidization velocity. The agglomerates are located at the bottom of the bed in Figure 2.8. The simulation has segregation where the agglomerates travel downwards in the bed. The segregation may be the reason that the two figures show such similarities without using the same particle size for the bed, agglomerate size, and process temperature.

Figure 6.16 and Figure 6.17 shows an indication that the bed with agglomerates do not completely fluidize. Figure 6.16 shows well-distributed voids over the column, while Figure 6.17 shows that the voids are more restricted and that there are zones where the bed is defluidized.

Figure 6.18, Figure 6.19, and Figure 6.20 displays the following: Agglomerates position in the bed, how the bed would have behaved without agglomerates, and how it is behaving with agglomerates. Figure 6.20 also shows an indication that channeling is occurring in the bed because of the agglomerates.

Figure 6.21 and Figure 6.22 shows that at the velocity of 0.37 m/s, the bed is turbulent/sluggish and that most of the agglomerates are at the bottom while the bed particles are at the top.

It is clearly shown in the figures which include agglomerates, that they prevent the fluidized bed from providing the advantages it is supposed to have. These advantages are a well-mixed solid-fluid contact for the biomass and to create a uniform temperature distribution in the bed.



## 6 Results and Discussion

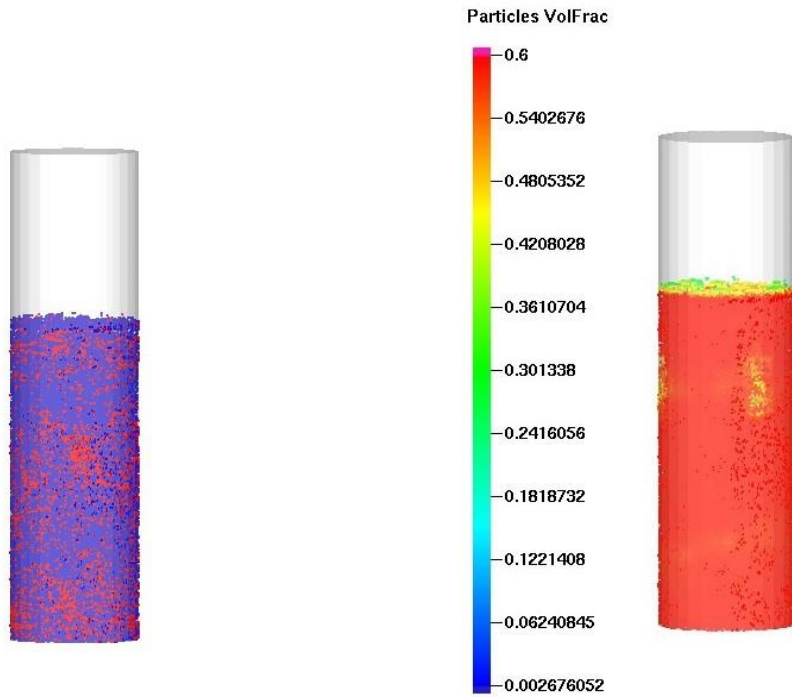


Figure 6.14: Result, Pilot-Scale Gasifier: species at minimum fluidization velocity of 0.055 m/s.

Figure 6.15: Result, Pilot-Scale Gasifier: particle volume fraction at minimum fluidization velocity of 0.055 m/s.

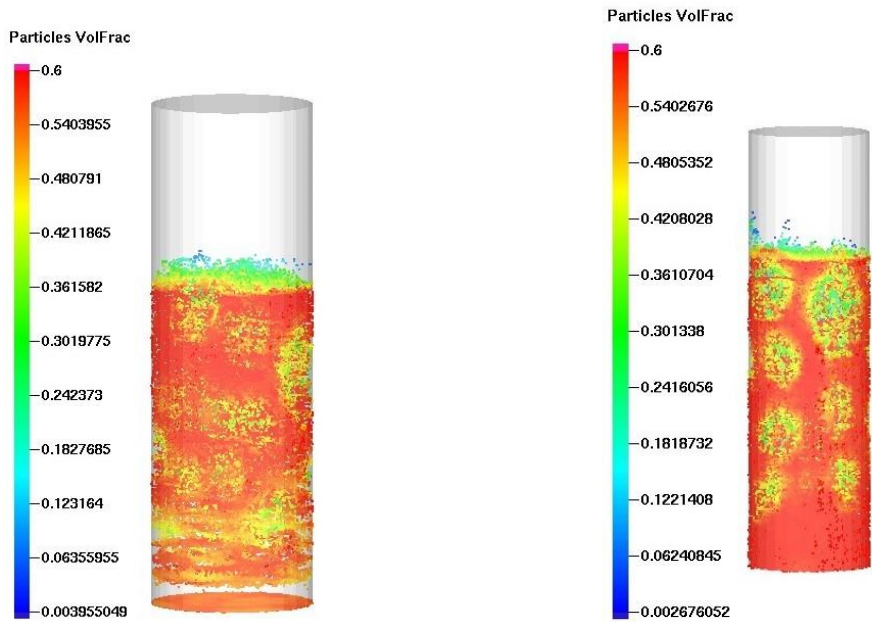


Figure 6.16: Result, Pilot-Scale Gasifier: particle volume fraction without agglomerates at a gas velocity of 0.085 m/s

Figure 6.17: Result, Pilot-Scale Gasifier: particle volume fraction with agglomerates at a gas velocity of 0.085 m/s

## 6 Results and Discussion



Figure 6.18: Result, Pilot-Scale Gasifier: at a gas velocity of 0.101 m/s.

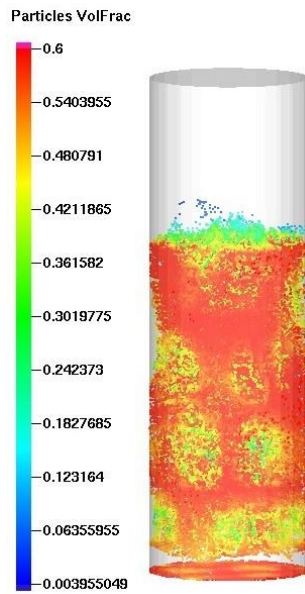


Figure 6.19: Result, Pilot-Scale Gasifier: particle volume fraction without agglomerates at a gas velocity of 0.101 m/s.

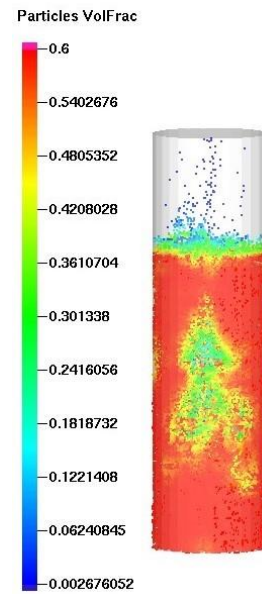


Figure 6.20: Result, Pilot-Scale Gasifier: particle volume fraction, at a gas velocity of 0.101 m/s.



Figure 6.21: Result, Pilot-Scale Gasifier: at a gas velocity of 0.37 m/s.

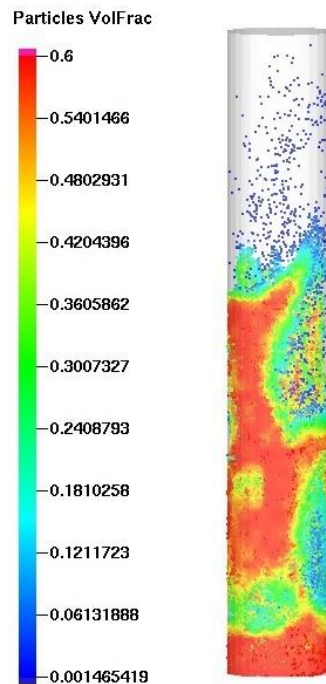


Figure 6.22: Result, Pilot-Scale Gasifier: particle volume fraction, at a gas velocity of 0.37 m/s.

## 7 Conclusion

The main goal was to develop a CPF model that could simulate the bubbling fluidized bed's flow behavior with agglomerates. To reach this main goal, there were sub-goals such as literature review, experiments, drag model testing, parameter testing, scaling, and agglomerate injections.

The CPF model was created in Barracuda VR 17.4.1. The model was tested and compared with experimental data from both a cold BFB and a hot BFB. The tests included different drag models and software parameters. The model was validated to use the Wen-Yu drag model with a timestep of 0.0001 s. The model provided an average deviation of 6 % between the experimental and the simulated pressure gradient for the cold BFB. The hot BFB had only one comparable point, which gave a deviation of 3 %. The deviation for minimum fluidization velocity between the experimental results and the simulation for cold and hot BFB was 6 % and 12 %, respectively.

The hot BFB geometry was scaled up with the use of Glicksman's rules, where the dimensionless parameter  $L/d_p$  was neglected. The simulated pilot-scale gasifier gave a deviation of 55 % between the simulated and the calculated Glicksman's  $u_{mf}$ . The scale was accepted due to simplicity and the needed size for maintaining the same grid resolution throughout the two gasifier scales. The scaling factor for the up-scaling was 5, which gave 0.5 m in diameter and 5 m in height for the pilot-scaled gasifier. The grid has 10000 uniformly distributed cubed cells that correspond to the physical size of 5 cm in all directions.

The agglomerate injection showed that as an additional entity in the bed, an amount that corresponds to 20 % of the bed volume was needed for the fluidized bed to change its flow behavior. The agglomerates used in the simulation have a size of 3-4 cm in diameter and a density of 1506 kg/m<sup>3</sup>. Sand with a density of 2650 kg/m<sup>3</sup> was used as bed material in all the experiments.

The simulation of an agglomerated bed, where agglomerates are an additional entity, showed similar behavior in the bed as with experimental data found in the literature. The similarities are when the agglomerates are located at the bottom of the bed. The flow behavior in the fluidized bed was affected when introduced to agglomerates, and the parameters in the bed changed. The overall pressure gradient in the bed decreased, while the minimum fluidization velocity increased. The bed showed signs of segregation, fluid channeling, and defluidized zones, thus making the bed not capable of complete fluidization. The changes in the fluidized bed flow behavior are negatively impacting the fluidization properties in the bed, such as good contact between particles and fluid, and the possibility to have uniform-temperature in the bed.

For further study on the simulation model, it is recommended to test the drag model parameters for the possibility of increasing the CPF model accuracy. Experimentally find the minimum fluidization velocity in the hot BFB. Experimentally validate the agglomerated bed simulation data. Experimentally validate the PSD test. Perform a test with different initial bed locations for the agglomerates and cross-check the simulated data with literature data or experimental data. It is also recommended to test the chemistry section in Barracuda to create a more realistic agglomeration formation. Where the agglomerates are formed through chemical reactions instead of being added as an additional entity in the bed, the validated CPF model may be suitable to use in this case.

# References

- [1] "Viaspace : Biomass Versus Fossil Fuels, Solar and Wind", *Viaspace.com*, 2020. [Online]. Available: [https://www.viaspace.com/biomass\\_versus\\_alternatives.php](https://www.viaspace.com/biomass_versus_alternatives.php). [Accessed: 08- Feb- 2020]
- [2] R. Cho, "Is Biomass Really Renewable?", *State of the Planet*, 2020. [Online]. Available: <https://blogs.ei.columbia.edu/2011/08/18/is-biomass-really-renewable/>. [Accessed: 08- Feb- 2020]
- [3] "Biomass explained - U.S. Energy Information Administration (EIA)", *Eia.gov*, 2018. [Online]. Available: <https://www.eia.gov/energyexplained/biomass/>. [Accessed: 22- Apr- 2020]
- [4] "Gasification | Student Energy", *Studentenergy.org*. [Online]. Available: <https://www.studentenergy.org/topics/gasification>. [Accessed: 22- Apr- 2020]
- [5] P. Basu, *Biomass gasification, pyrolysis and torrefaction*, 2nd ed. Elsevier Inc, 2013.
- [6] L. Rosendahl, *Biomass combustion, technology and engineering*. Sawston: Woodhead Publishing, 2013.
- [7] C. Higman and M. Van der Burgt, *Gasification*, 2nd ed. Burlington: Gulf Professional Publishing, 2008.
- [8] G. Brown, A. Hawkes, A. Bauen, and M. Leach, "1. Biomass Applications," *Centre for Energy Policy and Technology, Imperial College*, 2005
- [9] R. K. Thapa, "Optimization of flow behavior in biomass gasification reactor", 2015
- [10] S. Thapa, "Study on ash melting behavior in the biomass gasification reactor", 2019
- [11] A. Croxford and M. Gilbertson, "Pressure fluctuations in bubbling gas-fluidized beds", *Chemical Engineering Science*, vol. 66, no. 16, pp. 3569-3578, 2011.
- [12] C. Lin and M. Wey, "Statistical and power spectral analysis of quality of fluidization for different particle size distributions at high temperature", *Advanced Powder Technology*, vol. 15, no. 1, pp. 79-96, 2004.
- [13] D. Kunii, O. Levenspiel and H. Brenner, *Fluidization Engineering*, 2nd ed. Stoneham: Butterworth-Heinemann, 1991.
- [14] D. Gidaspow, *Multiphase Flow and Fluidization*. London: ACADEMIC PRESS LIMITED, 1994.
- [15] N. Furuvik, "Flow behavior in an agglomerated fluidized bed gasifier".
- [16] N. Furuvik, R. Jaiswal, R. Thapa and B. Moldestad, "CPFD model for prediction of flow behavior in an agglomerated fluidized bed gasifier", *International Journal of Energy Production and Management*, vol. 4, no. 2, pp. 105-114, 2019.
- [17] M. Bartels, W. Lin, J. Nijenhuis, F. Kapteijn and J. van Ommen, "Agglomeration in fluidized beds at high temperatures: Mechanisms, detection and prevention", *Progress in Energy and Combustion Science*, vol. 34, no. 5, pp. 633-666, 2008.

## References

- [18] A. Montes, "Factors Affecting Bed Agglomeration in Bubbling Fluidized Bed Biomass Boilers", *Electronic Thesis and Dissertation Repository*, 2014 [Online]. Available: <https://ir.lib.uwo.ca/etd/2325>. [Accessed: 07- Mar- 2020]
- [19] L. Glicksman, "Scaling relationships for fluidized beds", *Chemical Engineering Science*, vol. 39, no. 9, pp. 1373-1379, 1984.
- [20] L. Glicksman, M. Hyre and K. Woloshun, "Simplified scaling relationships for fluidized beds", *Powder Technology*, vol. 77, no. 2, pp. 177-199, 1993.
- [21] L. Glicksman, M. Hyre and P. Farrell, "Dynamic similarity in fluidization", *International Journal of Multiphase Flow*, vol. 20, pp. 331-386, 1994.
- [22] T. Basmoen, C. Deeraska, C. Nwosu, E. Qaredaghi, R. Jaiswal, N. Furuvik and B. Moldestad, "Experimental and computational studies on biomass gasification in fluidized beds", *International Journal of Energy Production and Management*, vol. 4, no. 2, pp. 168-177, 2019.
- [23] "File:Laboratory sieves BMK.jpg - Wikimedia Commons", *Commons.wikimedia.org*, 2020. [Online]. Available: [https://commons.wikimedia.org/wiki/File:Laboratory\\_sieves\\_BMK.jpg](https://commons.wikimedia.org/wiki/File:Laboratory_sieves_BMK.jpg). [Accessed: 22- Apr- 2020]
- [24] "Vibratory Sieve Shaker AS 200 Control 100-240 V, 1 Phase, 50/60 Hz", *Preiser Scientific- Coal Testing, Water Testing, General Laboratory, Calorimeter*, 2020. [Online]. Available: <https://www.preiser.com/vibratorysieveshakeras200basic120v1phase60hz-1.aspx>. [Accessed: 22- Apr- 2020]
- [25] D. Sathiyamoorthy and M. Horio, "On the influence of aspect ratio and distributor in gas fluidized beds", *Chemical Engineering Journal*, vol. 93, no. 2, pp. 151-161, 2003.
- [26] C. Agu, C. Pfeifer, M. Eikeland, L. Tokheim and B. Moldestad, "Measurement and characterization of biomass mean residence time in an air-blown bubbling fluidized bed gasification reactor", *Fuel*, vol. 253, pp. 1414-1423, 2019.
- [27] C. Crowe, J. Schwarzkopf, M. Sommerfeld and Y. Tsuji, *Multiphase flows with droplets and particles*, 2nd ed. Boca Raton, FL: CRC Press, 2011.
- [28] *Barracuda Virtual Reactor User Manual. CPDFD Software [Online]. Available: https://cpfd-software.com/customer-support. [Accessed: 04- May- 2020]*
- [29] "Barracuda® Computational Particle Fluid Dynamics (CPFD®) Software", *Energy.gov*, 2020. [Online]. Available: <https://www.energy.gov/eere/amo/barracuda-computational-particle-fluid-dynamics-cpfd-software>. [Accessed: 22- Apr- 2020]
- [30] R. Niven, "Physical insight into the Ergun and Wen & Yu equations for fluid flow in packed and fluidised beds", *Chemical Engineering Science*, vol. 57, no. 3, pp. 527-534, 2002.
- [31] R. Turton and O. Levenspiel, "A short note on the drag correlation for spheres", *Powder Technology*, vol. 47, no. 1, pp. 83-86, 1986.
- [32] R. Chhabra, L. Agarwal and N. Sinha, "Drag on non-spherical particles: an evaluation of available methods", *Powder Technology*, vol. 101, no. 3, pp. 288-295, 1999.

# Appendices

## Appendix A Task Description

Faculty of Technology, Natural Sciences and Maritime Sciences

### FMH606

**Title:** Ash melting and agglomeration in fluidized bed gasification of biomass

**USN supervisors:** Prof. Britt M. E. Moldestad, Nora C. I. S. Furuvik

**Task background:**

The global energy demand has increased over the last decades, and there is an urgent need to promote the use of sustainable alternatives to fossil fuels in order to limit the Earth's global warming. Among the different available energy sources, biomass is the key resource to reduce the dependence of fossil fuels, and at the same time provide energy in a sustainable manner. One of the promising conversion technologies for biomass is fluidized bed gasification, which involves heating and converting of the biomass into a gaseous mixture of syngas.

Fluidized beds offer distinct advantages over other conversion technologies. However, ash related problems are the main obstacles to successful applications of fluidized bed biomass gasification. Generally, these problems are associated with the formation of melted ash, which forms agglomerates that deposit at high temperatures. The agglomeration process is a result of interaction between the bed material and alkali metals present in the biomass ash. The fluidized bed's behavior is affected by the agglomeration

Experimental work and CPFD-modelling can be combined in order to achieve a better understanding of the bubbling fluidized bed behavior when presented with agglomerates.

**Task description:**

The project will focus on:

- (a) Literature study on gasification, operating parameter, and flow behavior when there are agglomerates in a bubbling fluidized bed.
- (b) Experimental study of the flow characteristics in a hot and cold bubbling fluidized bed.
- (c) CPFD-simulations to predict the flow behavior in an agglomerated bed.

**Student category:** PT or EET students. It is beneficial to have some knowledge about fluidization.

**Practical arrangements:**

Necessary software for CPFD-simulations will be provided by USN.  
Experimental equipment and analysis instruments are located at USN.

**Signatures:**

Supervisor (date and signature):

26.05.2020 *Britt Moldestad*

Student (write clearly in all capitalized letters):

*KRISTER JAKOBSEN*

Student (date and signature):

*26/05-20 Krister Jakobsen*

Appendix B Sieve Analysis For Both The Fluidized Beds

<b>Sieve Range (µm)</b>	<b>Mean size (µm)</b>	<b>WF</b>	<b>WF / Diameter</b>
<b>300-355</b>	328	0.079	2.4e-4
<b>355-425</b>	390	0.088	2.3e-4
<b>425-500</b>	463	0.076	1.7e-4
<b>500-600</b>	550	0.261	4.7e-4
<b>600-700</b>	650	0.496	7.6e-4

Sieve analysis for Cold-BFB

<b>Sieve Range (µm)</b>	<b>Mean size (µm)</b>	<b>Weight Fraction</b>	<b>Weight / Diameter</b>
<b>200-300</b>	250	0.286	1.1e-3
<b>300-425</b>	363	0.274	7.5e-4
<b>425-500</b>	463	0.101	2.2e-4
<b>500-600</b>	550	0.291	5.3e-4
<b>600-700</b>	650	0.048	7.3e-5

Sieve analysis for BFB-gasifier

Appendix C Cumulative Spread Sheet Used In Barracuda For PSD Testing

Mean Particle size

Weight frac (%)	Cumulative (%)	Size (um)	Radius (m)
0	0	300	0.00015
0	0.00	355	0.000178
0	0.00	535	0.000268
100	100.00	500	0.00025
0	100.00	600	0.0003
0	100.00	700	0.00035

High Cumulative Percentage

Weight frac (%)	Cumulative (%)	Size (um)	Radius (m)
0	0	300	0.00015
0	0.00	355	0.000178
0	0.00	425	0.000213
25	25.00	500	0.00025
50	75.00	600	0.0003
25	100.00	700	0.00035

Low Cumulative Percentage

Weight frac (%)	Cumulative (%)	Size (um)	Radius (m)
0	0	300	0.00015
25	25.00	355	0.000178
50	75.00	425	0.000213
25	100.00	500	0.00025
0	100.00	600	0.0003
0	100.00	700	0.00035



Appendix D Velocity Profile Used in Cases: Confirming the Scaling, extended flow BC for BFB-gasifier, and Simulating with Agglomerates

<i>Time</i> [s]	Velocity $\left[\frac{m}{s}\right]$	<i>Time</i> [s]	Velocity $\left[\frac{m}{s}\right]$	<i>Time</i> [s]	Velocity $\left[\frac{m}{s}\right]$	<i>Time</i> [s]	Velocity $\left[\frac{m}{s}\right]$
0	0.015	80	0.101	0	0.015	65	0.08
5	0.02	85	0.135	5	0.02	70	0.085
10	0.025	90	0.168	10	0.025	75	0.09
15	0.03	95	0.202	15	0.03	80	0.101
20	0.035	100	0.235	20	0.035	85	0.135
25	0.04	105	0.269	25	0.04	90	0.168
30	0.045	110	0.303	30	0.045	95	0.202
35	0.05	115	0.336	35	0.05	100	0.235
40	0.055	120	0.370	40	0.055	105	0.269
45	0.06	125	0.403	45	0.06	110	0.303
50	0.065	130	0.437	50	0.065	115	0.336
55	0.07	135	0.471	55	0.07	120	0.370
60	0.075	140	0.504	60	0.075		
65	0.08	145	0.538				
70	0.085	150	0.572				
75	0.09						

The flow BC used when confirming the scaling

The flow BC used when simulating with agglomerates

## Appendices

Flow BC used when locating the minimum fluidization velocity for the BFB-gasifier

<i>Time</i> [s]	<i>Velocity</i> $\left[\frac{m}{s}\right]$	<i>Time</i> [s]	<i>Velocity</i> $\left[\frac{m}{s}\right]$
0	0.005	50	0.120
5	0.020	55	0.135
10	0.015	60	0.150
15	0.030	65	0.165
20	0.045	70	0.180
25	0.052	75	0.196
30	0.060	80	0.211
35	0.075	85	0.226
40	0.090	90	0.241
45	0.105	95	0.256

Appendix E Graphs and Simulation results.

